ACADEMIC PRESS

Available online at www.sciencedirect.com

SCIENCE DIRECT®

Journal of Computational Physics 185 (2003) 309–341

JOURNAL OF COMPUTATIONAL PHYSICS

www.elsevier.com/locate/jcp

# Shock capturing, level sets, and PDE based methods in computer vision and image processing: a review of Osher's contributions

Ronald P. Fedkiw [a,1], Guillermo Sapiro [b,2], Chi-Wang Shu [c,*,3]

[a] *Department of Computer Science, Stanford University, Stanford, CA 94305, USA*
[b] *Department of Electrical and Computer Engineering, University of Minnesota, Minneapolis, MN 55455, USA*
[c] *Division of Applied Mathematics, Brown University, 182 George Street Box F, Providence, RI 02912, USA*

Received 11 December 2001; received in revised form 4 September 2002; accepted 27 September 2002

**Abstract**

In this paper we review the algorithm development and applications in high resolution shock capturing methods, level set methods, and PDE based methods in computer vision and image processing. The emphasis is on Stanley Osher's contribution in these areas and the impact of his work. We will start with shock capturing methods and will review the Engquist–Osher scheme, TVD schemes, entropy conditions, ENO and WENO schemes, and numerical schemes for Hamilton–Jacobi type equations. Among level set methods we will review level set calculus, numerical techniques, fluids and materials, variational approach, high codimension motion, geometric optics, and the computation of discontinuous solutions to Hamilton–Jacobi equations. Among computer vision and image processing we will review the total variation model for image denoising, images on implicit surfaces, and the level set method in image processing and computer vision.


*Keywords:* Shock capturing method; Level set method; Computer vision; Image processing

* Corresponding author. Tel.: 1-401-863-2549; fax: 1-401-863-1355.
*E-mail addresses:* fedkiw@cs.stanford.edu (R.P. Fedkiw), guille@mail.ece.umn.edu (G. Sapiro), shu@cfm.brown.edu (C.-W. Shu).
[1] Research supported in part by an ONR YIP and PECASE award N00014-01-1-0620, NSF DMS-0106694, and NSF ACI-0121288.
[2] Research supported by the Office of Naval Research, the Office of Naval Research Young Investigator Award, the Presidential Early Career Awards for Scientists and Engineers (PECASE), a National Science Foundation CAREER Award, and the National Science Foundation Learning and Intelligent Systems Program (LIS).
[3] Research supported by ARO grant DAAD19-00-1-0405, NSF Grants DMS-9804985, ECS-9906606, and DMS-0207451, NASA Langley grant NCC1-01035 and AFOSR Grant F49620-02-1-0113.

0021-9991/03/$ - see front matter 
doi:10.1016/S0021-9991(02)00016-5

## 1. Introduction

This paper is written on the occasion of Stanley Osher's 60th birthday and serves as a review paper on a few selected areas in high resolution shock capturing schemes, level set methods, and PDE based methods in computer vision and image processing. The emphasis is on Stanley Osher's contribution in these areas and the impact of his work.

Shock capturing numerical methods have seen revolutionary developments over the past 20 years. These are methods which deal with the numerical solutions of PDEs with discontinuous solutions. Such PDEs include nonlinear hyperbolic systems such as Euler equations of compressible gas dynamics. The problems are difficult because traditional linear numerical methods are either too diffusive, or give unphysical oscillations near the discontinuities which can lead to nonlinear instabilities. The class of high resolution numerical methods overcomes this difficulty to a large extent.

Level set methods have seen tremendously expanded applications in many areas over the past 15 years. This has been made possible by the flexibility of the level set formulation in dealing with dynamic evolutions and topological changes of curves and surfaces, and by the mathematical theory and numerical tools developed in the past 15 years in studying these methods.

PDE based methods in computer vision and image processing have been actively studied in the past few years. Again, the rapid development of mathematical models, solution tools such as level set methods, and high resolution numerical schemes has made PDE based method one of the major tools in computer vision and image processing.

Stanley Osher has made influential contributions to all these fields. A distinctive feature of his research is that he emphasizes both fundamental problems in algorithm design and analysis, and practical considerations for the applications of the algorithms. This seems also to be the objective of the Journal of Computational Physics. It is thus not a surprise that a significant portion of Osher's journal publications have appeared in the Journal of Computational Physics. This is particularly the case for Osher's work over the past 15 years. Osher's work has been highly influential, an indication of this being the citation statistics. For example, according to the ISI database, which lists papers in selected journals of high impact since 1975, the 87 papers of Osher listed there have been collectively cited about 2500 times (as on July 1, 2002, the same below). Among these, 12 papers have been cited over 100 times each. The top four highly cited papers of Osher include the paper of Osher and Sethian [145] on level set methods, cited 538 times; the paper of Harten et al. [78] on ENO schemes, cited 314 times; and the two papers of Shu and Osher [168,169] on ENO schemes, cited 251 and 250 times, respectively. We remark that all these four papers were published in the Journal of Computational Physics.

The organization of this paper is as follows. Section 2 is devoted to high resolution shock capturing methods for problems with discontinuous or otherwise nonsmooth solutions. Section 3 contains a review of the very popular level set methods. In Section 4 we address PDE based methods in computer vision and image processing, and finally in Section 5 we give some concluding remarks.

Before ending this section, we remark that early in his career, Osher did a lot of research on the study of linear stability for finite difference and other numerical methods for hyperbolic, parabolic, and other types of PDEs, especially those for initial-boundary value problems. This includes for example the work in [127] which followed up on a seminal paper of Kreiss [100] and used Toeplitz matrices in an elegant way to derive what was later called the GKS condition [73], and the work in [128] where stability conditions for initial-boundary value problems for parabolic equations were obtained, generalizing the work of Varah [186]. In [111], Majda and Osher extended Kreiss' well posedness condition for initial-boundary value problems for hyperbolic equations to those with uniformly characteristic boundaries. In [110], Majda and Osher analyzed the reflection of singularities at the boundary for nongrazing reflection for hyperbolic equations. In [112], Majda and Osher showed how error propagates globally within the domain of dependence for numerical approximations to coupled hyperbolic systems. The paper by Majda et al. [109] was the first to

recommend the use of smooth cutoff functions on the frequency domain for spectral methods to confine errors to local regions near propagating discontinuities and for stability. Sharp estimates on the region of propagation were obtained. These cutoffs are now widely used in the literature and the paper is still frequently cited, 45 times total, including many in recent years. Finally, in [49], Engquist et al. obtained wavelet based fast algorithms for linear hyperbolic and parabolic equations, and in [46,55,56], Engquist et al. considered numerical methods for high frequency asymptotics for geometric optics. These might be considered nonlinear, since the eikonal equation is. We shall not review in detail these early works of Osher on linear methods in the remaining part of this paper, as they are less directly related to the objectives of JCP.

## 2. High resolution shock capturing methods

Shock capturing methods refer to a class of numerical methods for solving problems containing discontinuities (shocks, contact discontinuities, or other discontinuities), which can automatically "capture" these discontinuities without special effort to track them. A typical situation would be the solution of a hyperbolic conservation law, either a scalar equation or a system, either in one spatial dimension

$$u_t + f(u)_x = 0 \tag{2.1}$$

or in multiple (say three) spatial dimensions

$$u_t + f(u)_x + g(u)_y + h(u)_z = 0. \tag{2.2}$$

A well-known system of conservation laws is the Euler equations for inviscid fluid flow dynamics. The Euler equations are rather interesting because the presence of discontinuities forces one to consider weak solutions where the derivatives of solution variables can fail to exist. While a contact discontinuity is essentially linear, the nonlinear nature of a shock wave discontinuity allows it to develop as the solution progresses forward in time even if the data are initially smooth. A main ingredient of shock capturing methods is the conservation form of a scheme, namely, a scheme approximating (2.1) is in the form

$$\frac{\mathrm{d}u_j}{\mathrm{d}t} + \frac{1}{\Delta x}\left(\hat{f}_{j+\frac{1}{2}} - \hat{f}_{j-\frac{1}{2}}\right) = 0, \tag{2.3}$$

where $u_j$ is an approximation to either the point value $u(x_j,t)$ or the cell average $\bar{u}(x_j,t) = (1/\Delta x)\int_{x_j-(\Delta x/2)}^{x_j+(\Delta x/2)} u(x,t)\,\mathrm{d}x$ of the exact solution of (2.1), and $\hat{f}_{j+\frac{1}{2}}$ is a numerical flux which typically depends on a few neighboring points

$$\hat{f}_{j+\frac{1}{2}} = \hat{f}(u_{j-k}, u_{j-k+1}, \ldots, u_{j+m})$$

and satisfies the following two conditions: it is consistent with the physical flux $f(u)$ in the sense $\hat{f}(u,u,\ldots,u) = f(u)$, and it is at least Lipschitz continuous with respect to all its arguments. Notice that (2.3) is written in a semi-discrete method of lines form, while in practice the time variable $t$ must also be discretized. Conservative schemes in the form of (2.3) are especially suitable for computing solutions with shocks, because of the important Lax–Wendroff theorem, which states that solutions to such schemes, if convergent, would converge to a weak solution of (2.1). In particular, this means that the computed shocks will propagate with the correct speed. Almost all shock capturing schemes, including those developed by Osher and his collaborators, are of the conservation form (2.3). However, there are certain situations where a relaxation on the strict conservation would be beneficial and would not hurt the convergence to weak solutions under suitable additional assumptions. The work of Osher and Chakravarthy [134] on the

"weak conservation form" for schemes on general curvilinear coordinates, and the work of Fedkiw et al. [60] on "ghost fluid" method, which treats the fluid interface in a nonconservative fashion, are such examples.

### 2.1. First order monotone schemes

In the late 1970s and early 1980s, designing good first order monotone schemes for (2.1) and (2.2), which give monotone shock transitions and can be proven to converge to the physically relevant weak solutions (e.g. [39]), was an active research area. The Godunov scheme is a scheme with the least numerical dissipation among first order monotone schemes, however it is costly to evaluate for complex flux functions $f(u)$, and its flux is only Lipschitz continuous but not smoother. The Lax–Friedrichs scheme is easy to evaluate and very smooth but is excessive dissipative.

In [47,48], Engquist and Osher designed monotone schemes for the transonic potential equations and for general scalar conservation laws, which are relatively easy to evaluate, are $C^1$ smooth, and have a small dissipation almost comparable with Gudonov schemes. The main idea is to approximate everything by rarefaction waves (multi-valued solutions suitably integrated over for shocks). These Engquist–Osher schemes soon became very popular, especially for implicit type methods and steady state calculations, for which the extra smoothness of the numerical fluxes helped a lot. Similar schemes for Hamilton–Jacobi equations were given by Osher and Sethian [145].

Later, Osher [129] and Osher and Solomon [147] generalized these schemes to systems of conservation laws, obtaining what was later referred to as the Osher scheme in the literature. The Osher scheme for systems has a closed form formula (for Euler equations of gas dynamics and many other systems), hence no iterations are needed, unlike the Godunov scheme. It is smoother ($C^1$) than the Godunov scheme and also has smaller dissipation than the simpler Lax–Friedrichs scheme. Applications of the Osher scheme to the Euler equations can be found in Chakravarthy and Osher [24].

In [143], Osher and Sanders designed a conservative procedure to handle locally varying time and space grids for first order monotone schemes, and proved convergence to entropy solutions for such schemes. These ideas have been used later by Berger and Colella on their adaptive methods, e.g. [9].

### 2.2. High resolution TVD schemes

First order monotone schemes are certainly nice in their stability and convergence to the correct entropy solutions, however they are too diffusive for most applications. One would need to use many grid points to get a reasonable resolution, which seriously restricts their usefulness for multi-dimensional simulations.

In the 1970s and early and mid 1980s, the so-called "high resolution" schemes, i.e., those schemes which are at least second order accurate and are stable when shocks appear, were developed. These started with the earlier work of, e.g., the FCT methods of Boris and Book [13], and the MUSCL schemes of van Leer [185], and moved to Harten's TVD schemes [77]. Osher and his collaborators did extensive research on TVD schemes, and contributed significantly towards the analysis of such methods, during this period. These include the schemes developed and analyzed in [131,132,135], and the very high order (measured by truncation errors in smooth, monotone regions) TVD schemes in [136].

### 2.3. Entropy conditions

The entropy condition is an important feature for conservation laws. Because weak solutions are not unique, entropy conditions are needed to single out a unique, physically relevant solution. Osher and his collaborators did extensive research on designing and analyzing entropy condition satisfying numerical methods for conservation laws.

In [113], Majda and Osher proved that the traditional second order Lax–Wendroff scheme, although linearly stable, is not $L^2$ stable when solving nonlinear conservation laws with discontinuous solutions. They then provided a recipe of adding artificial viscosities, such that the scheme maintained second order accuracy yet could be proven convergent to the entropy solution. This scheme is however oscillatory, hence not very practical in applications.

In [131], Osher provided a general framework to study systematically entropy conditions for numerical schemes. This was followed by the work of Osher and Chakravarthy [135] in the study of high resolution schemes and entropy conditions, the work of Osher [132] on generalized MUSCL schemes, the work of Osher and Tadmor [148] on entropy condition and convergence of high resolution schemes, and the work of Brenier and Osher [14] on entropy condition satisfying "maxmod" second order schemes. Entropy condition satisfying approximations for the full potential equation of transonic flow were given in [140].

### 2.4. ENO schemes

In the mid 1980s it was realized that TVD schemes, despite their excellent stability and high resolution properties, have serious deficiency in that they degenerate to first order at *smooth* extrema of the solution [135]. Thus, even though TVD schemes can be designed to any order of accuracy, see for example the schemes up to 13th order accurate in [136], practical TVD schemes are referred to as second order schemes since the global $L^1$ errors of any TVD scheme can only be second order, even for smooth, nonmonotone solutions.

In [79], Harten and Osher relaxed the TVD restriction, and replaced it by a UNO restriction, in that the total number of numerical extrema does not increase and their amplitudes could be allowed to increase slightly. The UNO scheme in [79] is uniformly second order accurate including at smooth extrema. However, it was soon realized that the UNO restriction was still too strong and excluded schemes of higher than second order. Thus, the concept of ENO, or essentially nonoscillatory, schemes was first given by Harten et al. [78] in 1987. The clever idea is that of an adaptive stencil, which is chosen based on the local smoothness of the solution, measured by the Newton divided differences of the numerical solution. Thus the order of accuracy of the scheme is never reduced, however the local stencil automatically avoids crossing discontinuities. Such schemes allow both the number of numerical extrema and their amplitudes to increase, however such additional oscillations are controlled on the level of truncation errors even if the solution is not smooth. ENO schemes have been extremely successful in applications, because they are simple in concept, allow arbitrary orders of accuracy, and generate sharp, monotone (to the eye) shock transitions together with high order accuracy in smooth regions of the solution including at the extrema.

The original ENO schemes in [78] are in the cell averaged form, namely they are finite volume schemes approximating an integrated version of (2.1). Finite volume schemes have the advantage of easy handling of nonuniform meshes and general geometry in multi-space dimensions, however they are extremely costly in multi-space dimensions, when the order of accuracy is higher than 2, because then it is not possible to equate cell averages with point values, as they only agree up to second order accuracy, and a complex reconstruction procedure is needed to obtain point values from cell averages for evaluating the numerical fluxes. The cost is also associated with the high order numerical quadratures needed for evaluating the integration of the numerical fluxes along cell boundaries in multi-dimensions. Later, Shu and Osher [168,169], developed finite difference based ENO schemes using point values of the numerical solution, but still in conservation form (2.3). An important observation made in [168] and [169] is that the numerical flux $\hat{f}_{j+\frac{1}{2}}$ in (2.3) is *not* a high order approximation to the physical flux at $x_{j+\frac{1}{2}}$: the difference between the numerical flux $\hat{f}_{j+\frac{1}{2}}$ and the physical flux $f(u_{j+\frac{1}{2}})$ is $O(\Delta x^2)$. This is a common mistake among practitioners of finite difference schemes. If a high order interpolation on the point values $u_j$ is performed to obtain a high order approximation to $u_{j+\frac{1}{2}}$, and a numerical flux is chosen to approximate $f(u_{j+\frac{1}{2}})$ to a high order accuracy, then the scheme is only second order accurate. Correct choice of the numerical fluxes to obtain

arbitrarily high order accuracy is given in [168,169]. The approach in [169] is especially simple. A detailed description of the construction and comparison of finite volume and finite difference ENO schemes can be found in the lecture notes [167].

Also in [168], a class of nonlinearly stable high order Runge–Kutta time discretization methods is developed. Termed TVD time discretizations, these Runge–Kutta methods have become very popular and have been used in many schemes. See e.g. [69] for a review of such methods.

Analysis of ENO schemes was given in Harten et al. [80]. Applications of ENO schemes to 2D and 3D compressible flows, including turbulence and shear flow calculations, were given in Shu et al. [170]. Triangle based second order nonoscillatory schemes were given in Durlofsky et al. [42]. Nonoscillatory self-similar maximum principle satisfying high order shock capturing schemes were given in Liu and Osher [106]. Efficient characteristic projection in upwind difference schemes was given in Fedkiw et al. [63]. Convex ENO schemes without using field-by-field projection were given in Liu and Osher [107]. Chemically reactive flows were simulated in [62,179].

The popularity of ENO schemes is demonstrated by the citation statistics: among Osher's four most highly cited papers mentioned in the introduction, three of them are about ENO schemes, i.e. [78,168,169]. The top cited paper of Osher, [145], is on level set methods but also uses second order ENO schemes for the numerical solutions and is where the construction of ENO schemes for general Hamilton–Jacobi equations began.

### 2.5. WENO schemes

An improvement of ENO scheme is the WENO (weighted ENO) scheme, which was first developed by Liu et al. [108]. Both ENO and WENO use the idea of adaptive stencils in the reconstruction procedure based on the local smoothness of the numerical solution to automatically achieve high order accuracy and nonoscillatory property near discontinuities. ENO uses just one (optimal in some sense) out of many candidate stencils when doing the reconstruction; while WENO uses a convex combination of all the candidate stencils, each being assigned a nonlinear weight which depends on the local smoothness of the numerical solution based on that stencil. WENO improves upon ENO in robustness, better smoothness of fluxes, better steady state convergence, better provable convergence properties, and more efficiency.

WENO schemes have been further developed later by Jiang and Shu [90] for fifth order accurate finite difference schemes in one and several space dimensions, by Hu and Shu [82] and Shi et al. [166] for third and fourth order accurate finite volume schemes in two space dimensions using arbitrary triangulations, and by Balsara and Shu [6] on very high order WENO schemes. A detailed description can again be found in the lecture notes [167].

### 2.6. Hamilton–Jacobi equations

We will now move to the description of Osher's work in designing schemes for solving Hamilton–Jacobi equations. Further discussions on this topic will also be given in Section 3 on level set methods.

Consider the 1D Hamilton–Jacobi equation

$$\phi_t + H(\phi_x) = 0, \tag{2.4}$$

which becomes

$$(\phi_x)_t + H(\phi_x)_x = 0 \tag{2.5}$$

after taking a spatial derivative of the entire equation. Setting $u = \phi_x$ in Eq. (2.4) results in

$$u_t + H(u)_x = 0, \tag{2.6}$$

which is a scalar conservation law. Thus in one spatial dimension, a direct correspondence between Hamilton–Jacobi equations and conservation laws can be drawn. The solution $u$ to conservation law is the derivative of a solution $\phi$ to a Hamilton–Jacobi equation. Conversely, the solution $\phi$ to a Hamilton–Jacobi equation is the integral of a solution $u$ to a conservation law. This observation leads to a number of useful facts. For example, since the integral of a discontinuity is a kink (discontinuity in first derivative), solutions to Hamilton–Jacobi equations can develop kinks in the solution even if the data are initially smooth. In addition, solutions to Hamilton–Jacobi equations cannot generally develop a discontinuity (unless the corresponding conservation law solution develops a delta function). Thus, solutions $\phi$ to Eq. (2.4) are typically continuous. Furthermore, since conservation laws can have nonunique solutions, one needs to apply an entropy condition to pick out the "physically" relevant solution to Eq. (2.4).

Viscosity solutions for Hamilton–Jacobi equations were first proposed by Crandall and Lions [37] in order to pick out the physically relevant solution. In addition, monotone first order accurate numerical methods were first proven to converge by Crandall and Lions in [38]. In [130], Osher gave explicit formulas for solutions to the Riemann problems for nonconvex conservation laws and Hamilton–Jacobi equations. See also the multi-dimensional Riemann solver of Bardi and Osher [7]. These are important for numerical schemes such as Godunov schemes using such Riemann solvers as building blocks.

In [145], Osher and Sethian, in the context of discussing level set methods, provided a first order monotone scheme (an adaptation of the Engquist–Osher scheme [48]) and a second order ENO scheme based on the framework of Shu and Osher [168,169]. In [146], Osher and Shu developed high order ENO schemes for solving Hamilton–Jacobi equations, using various building blocks including the Lax–Friedrichs flux, the local Lax–Friedrichs flux, and the Roe flux with an entropy fix. In [101], Lafon and Osher developed high order 2D triangle based nonoscillatory schemes for solving Hamilton–Jacobi equations. Later, Jiang and Peng [89] designed WENO schemes for solving Hamilton–Jacobi equations on rectangular meshes and Zhang and Shu [195] designed WENO schemes for solving Hamilton–Jacobi equations on arbitrary triangular meshes. WENO scheme turns out to be very useful as the fifth order WENO scheme in [89] reduces the numerical errors by more than an order of magnitude over the third order accurate HJ ENO scheme on the same mesh for typical applications.

### *2.7. Additional topics*

Even though it does not exactly fit the title of this section, the work of Lagnado and Osher [102,103] is worth mentioning. These papers concern solving an inverse problem to compute the volatility in the European options Black–Scholes model, and they were the first to use PDE techniques to solve this inverse problem, via gradient descent and Tychonoff regularization, allowing the volatility, a coefficient in a parabolic equation to be a function of the independent variables, stock price and time. These papers have attracted a lot of attention after their publication.

Also worth mentioning is the work of Fatemi et al. [57] on using ENO schemes to solve the hydrodynamic models of semiconductor device simulations. This was the first work of using high order shock capturing methods in semiconductor device simulations, and has led to many further developments, e.g. [23,88].

## 3. Level set methods

Osher's most cited paper was [145], joint with Sethian, which introduced the level set method for dynamic implicit surfaces. The key idea was the Hamilton–Jacobi approach to numerical solutions of a time dependent equation for a moving implicit surface. The basic idea is as follows. Define an implicit surface as the zero isocontour of a function $\phi(\vec{x})$, and suppose that the velocity of each point on the implicit surface is

given by $\vec{V}(\vec{x})$. Given this velocity field, we wish to move all the points on the surface with this velocity. The simplest way to do this is to solve the ordinary differential equation

$$\frac{\mathrm{d}\vec{x}}{\mathrm{d}t} = \vec{V}(\vec{x}) \tag{3.1}$$

for every point $\vec{x}$ on the implicitly defined surface, i.e., for all $\vec{x}$ with $\phi(\vec{x}) = 0$. This is the Lagrangian formulation of the interface evolution equation. Since there is generally an infinite number of points on the front, this means discretizing the front into a finite number of pieces. For example, one could use segments in two spatial dimensions or triangles in three spatial dimensions. This is not so hard to accomplish if the connectivity does not change and the surface elements do not distort too much. Unfortunately, even the most trivial velocity fields can cause large distortion of boundary elements and the accuracy of the method can deteriorate quickly if one does not periodically modify the discretization in order to account for these deformations by smoothing and regularizing inaccurate surface elements. In order to avoid problems with instabilities, deformation of surface elements, and complicated surgical procedures for topological repair of interfaces, Osher and Sethian [145] proposed using the implicit function $\phi$ both to represent the interface and to evolve it. The evolution of the implicit function $\phi$ is governed by the simple convection equation

$$\phi_t + \vec{V} \cdot \nabla\phi = 0. \tag{3.2}$$

This is an Eulerian formulation of the interface evolution since the interface is captured by the implicit function $\phi$ as opposed to being tracked by interface elements as in a Lagrangian formulation. Eq. (3.2) is sometimes referred to as the level set equation. The velocity field given in Eq. (3.2) can come from a number of external sources. For example, when the $\phi(\vec{x}) = 0$ isocontour represents the interface between two different fluids, the interface velocity is calculated using the two-phase Navier–Stokes equations.

In general, one does not need to specify tangential components when devising a velocity field. Since the local unit normal to the interface, $\vec{N}$, and $\nabla\phi$ point in the same direction, $\vec{T} \cdot \nabla\phi = 0$ for any tangent vector $\vec{T}$ implying that the tangential velocity components vanish when plugged into the level set equation. For example, in two spatial dimensions with $\vec{V} = V_n\vec{N} + V_t\vec{T}$, the level set equation

$$\phi_t + \left(V_n\vec{N} + V_t\vec{T}\right) \cdot \nabla\phi = 0 \tag{3.3}$$

is equivalent to

$$\phi_t + V_n\vec{N} \cdot \nabla\phi = 0. \tag{3.4}$$

Furthermore, since

$$\vec{N} \cdot \nabla\phi = \frac{\nabla\phi}{|\nabla\phi|} \cdot \nabla\phi = \frac{|\nabla\phi|^2}{|\nabla\phi|} = |\nabla\phi|, \tag{3.5}$$

Eq. (3.4) can be rewritten as

$$\phi_t + V_n|\nabla\phi| = 0, \tag{3.6}$$

where $V_n$ is the component of velocity in the normal direction (the normal velocity). Eq. (3.6) is *also* known as the level set equation. Eq. (3.2) tends to be used for externally generated velocity fields while Eq. (3.6) tends to be used for (internally) self-generated velocity fields.

### 3.1. Level set calculus

In a series of papers that followed [145], Osher and coworkers introduced a level set calculus for the practical treatment of discretized implicit surfaces defined by time evolving partial differential equations.

We summarize some of the main points below, but refer the interested reader to the recent review article of Osher and Fedkiw [138] and the references within. In addition, we refer the reader to the books by Osher and Fedkiw [139] and by Sethian [163].

Suppose that the surface is implicitly defined as the zero isocontour of a function $\phi(\vec{x})$. Then the local sign of $\phi$ can be used to define the inside and outside regions of the domain. That is, $\vec{x}_0$ is inside the interface when $\phi(\vec{x}_0) < 0$, outside the interface when $\phi(\vec{x}_0) > 0$ and on the interface when $\phi(\vec{x}_0) = 0$. Implicit functions make simple Boolean operations easy to apply. If $\phi_1$ and $\phi_2$ are two different implicit functions, then $\phi(\vec{x}) = \min(\phi_1(\vec{x}), \phi_2(\vec{x}))$ is the implicit function representing the union of their interior regions. Similarly, $\phi(\vec{x}) = \max(\phi_1(\vec{x}), \phi_2(\vec{x}))$ represents the intersection of the interior regions. The complement of $\phi_1(\vec{x})$ is $\phi(\vec{x}) = -\phi_1(\vec{x})$, etc.

The gradient of the implicit function, $\nabla\phi$, is perpendicular to the isocontours of $\phi$ pointing in the direction of increasing $\phi$. Therefore, if $\vec{x}_0$ is a point on the zero isocontour of $\phi$, the local unit (outward) normal to the interface is

$$\vec{N} = \frac{\nabla\phi}{|\nabla\phi|} \tag{3.7}$$

for points on the interface. Eq. (3.7) can be used to define a function $\vec{N}$ everywhere on the domain embedding the normal in a function $\vec{N}$ that agrees with the normal for points on the interface. Similarly, the mean curvature of the interface is defined as the divergence of the normal

$$\kappa = \nabla \cdot \vec{N} \tag{3.8}$$

so that $\kappa > 0$ for convex regions, $\kappa < 0$ for concave regions, and $\kappa = 0$ for a plane.

The characteristic function $\chi^-$ of the interior region $\Omega^-$ is defined as

$$\chi^-(\vec{x}) = \begin{cases} 1 & \text{if } \phi(\vec{x}) \leqslant 0, \\ 0 & \text{if } \phi(\vec{x}) > 0, \end{cases} \tag{3.9}$$

where the boundary is arbitrarily included with the interior region. The characteristic function $\chi^+$ of the exterior region $\Omega^+$ is defined similarly as

$$\chi^+(\vec{x}) = \begin{cases} 0 & \text{if } \phi(\vec{x}) \leqslant 0, \\ 1 & \text{if } \phi(\vec{x}) > 0, \end{cases} \tag{3.10}$$

again including the boundary with the interior region. $\chi^\pm$ are functions of a multi-dimensional variable $\vec{x}$. It is often more convenient to work with functions of the scalar variable $\phi$. Thus, the 1D Heaviside function is defined as

$$H(\phi) = \begin{cases} 0 & \text{if } \phi \leqslant 0, \\ 1 & \text{if } \phi > 0, \end{cases} \tag{3.11}$$

where $\phi$ depends on $\vec{x}$ although it is not necessary to specify this dependence when working with $H$. Note that $\chi^+(\vec{x}) = H(\phi(\vec{x}))$ and $\chi^-(\vec{x}) = 1 - H(\phi(\vec{x}))$. The volume integral (area integral in $R^2$) of a function $f$ over the interior region $\Omega^-$ is defined as

$$\int_\Omega f(\vec{x})\chi^-(\vec{x})\mathrm{d}\vec{x}, \tag{3.12}$$

where the region of integration is all of $\Omega$ since $\chi^-$ prunes out the exterior region $\Omega^+$ automatically. The 1D Heaviside function can be used to rewrite this volume integral as

$$\int_\Omega f(\vec{x})(1 - H(\phi(\vec{x})))\mathrm{d}\vec{x} \tag{3.13}$$

representing the integral of $f$ over the interior region $\Omega^-$. Similarly,

$$\int_\Omega f(\vec{x})H(\phi(\vec{x}))\mathrm{d}\vec{x} \tag{3.14}$$

is the integral of $f$ over the exterior region $\Omega^+$.

By definition, the directional derivative of the Heaviside function $H$ in the normal direction $\vec{N}$ is the Dirac delta function

$$\hat{\delta}(\vec{x}) = \nabla H(\phi(\vec{x})) \cdot \vec{N}, \tag{3.15}$$

which is a function of the multi-dimensional variable $\vec{x}$. This distribution is only nonzero on the interface $\partial\Omega$ where $\phi = 0$. Eq. (3.15) can be rewritten as

$$\hat{\delta}(\vec{x}) = H'(\phi(\vec{x}))\nabla\phi(\vec{x}) \cdot \frac{\nabla\phi(\vec{x})}{|\nabla\phi(\vec{x})|} = H'(\phi(\vec{x}))|\nabla\phi(\vec{x})| \tag{3.16}$$

using the chain rule to take the gradient of $H$ and the definition of the normal from Eq. (3.7). In one spatial dimension, the delta function is defined as the derivative of the Heaviside function

$$\delta(\phi) = H'(\phi) \tag{3.17}$$

with $H(\phi)$ defined in Eq. (3.11) above. $\delta(\phi)$ is identically zero everywhere except where $\phi = 0$. Eq. (3.16) can be rewritten as

$$\hat{\delta}(\vec{x}) = \delta(\phi(\vec{x}))|\nabla\phi(\vec{x})| \tag{3.18}$$

using the 1D delta function $\delta(\phi)$. The surface integral (line integral in $R^2$) of a function $f$ over the boundary $\partial\Omega$ is defined as

$$\int_\Omega f(\vec{x})\hat{\delta}(\vec{x})\mathrm{d}\vec{x}, \tag{3.19}$$

where the region of integration is all of $\Omega$ since $\hat{\delta}$ prunes out everything except $\partial\Omega$ automatically. The 1D delta function can be used to rewrite this surface integral as

$$\int_\Omega f(\vec{x})\delta(\phi(\vec{x}))|\nabla\phi(\vec{x})|\mathrm{d}\vec{x}. \tag{3.20}$$

Typically, volume integrals are computed by dividing up the interior region, and surface integrals are computed by dividing up the boundary $\partial\Omega$. This requires treating a complex 2D surface in three spatial dimensions. By embedding the volume and surface integrals in higher dimensions, Eqs. (3.13), (3.14), and (3.20) avoid the need for identifying inside, outside or boundary regions. Instead the integrals are taken over the entire region $\Omega$.

Consider the surface integral in Eq. (3.20) where the 1D delta function needs to be evaluated. Since $\delta(\phi) = 0$ almost everywhere, i.e., except on the lower dimensional interface which has measure zero, it seems unlikely that any standard numerical approximation based on sampling will give a good approximation to this integral. Thus, a first order accurate smeared out approximation of $\delta(\phi)$ is used. First, a smeared out Heaviside function is defined as

$$H(\phi) = \begin{cases} 0, & \phi < -\epsilon, \\ \frac{1}{2} + \frac{\phi}{2\epsilon} + \frac{1}{2\pi}\sin\left(\frac{\pi\phi}{\epsilon}\right), & -\epsilon \leqslant \phi \leqslant \epsilon, \\ 1, & \epsilon < \phi, \end{cases} \tag{3.21}$$

where $\epsilon$ is a tunable parameter that determines the size of the bandwidth of numerical smearing. A typically good value is $\epsilon = 1.5\Delta x$ making the interface width equal to three grid cells when $\phi$ is normalized to a signed distance function with $|\nabla\phi| = 1$. Then the delta function is defined according to Eq. (3.17) as the derivative of the Heaviside function

$$\delta(\phi) = \begin{cases} 0, & \phi < -\epsilon, \\ \frac{1}{2\epsilon} + \frac{1}{2\epsilon}\cos\left(\frac{\pi\phi}{\epsilon}\right), & -\epsilon \leqslant \phi \leqslant \epsilon, \\ 0, & \epsilon < \phi, \end{cases} \tag{3.22}$$

where $\epsilon$ is determined as above. This delta function allows us to evaluate the surface integral in Eq. (3.20) using a standard sampling technique such as the midpoint rule. Similarly, the smeared out Heaviside function in Eq. (3.21) aids in the evaluation of the integrals in Eqs. (3.13) and (3.14).

A distance function $d(\vec{x})$ is defined as

$$d(\vec{x}) = \min|\vec{x} - \vec{x}_I| \quad \text{over all } \vec{x}_I \in \partial\Omega, \tag{3.23}$$

implying that $d(\vec{x}) = 0$ on the boundary where $\vec{x} \in \partial\Omega$. For a given point $\vec{x}$, suppose that $\vec{x}_C$ is the point on the interface closest to $\vec{x}$. The line segment from $\vec{x}$ to $\vec{x}_C$ is the shortest path from $\vec{x}$ to the interface. In other words, the path from $\vec{x}$ to $\vec{x}_C$ is the path of steepest descent for the function $d$. Evaluating $-\nabla d$ at any point on the line segment from $\vec{x}$ to $\vec{x}_C$ gives a vector that points from $\vec{x}$ to $\vec{x}_C$. Furthermore, since $d$ is Euclidean distance

$$|\nabla d| = 1. \tag{3.24}$$

A signed distance function is an implicit function $\phi$ with $\phi(\vec{x}) = d(\vec{x}) = 0$ for all $\vec{x} \in \partial\Omega$, $\phi(\vec{x}) = -d(\vec{x})$ for all $\vec{x} \in \Omega^-$, and $\phi(\vec{x}) = d(\vec{x})$ for all $\vec{x} \in \Omega^+$. Given a point $\vec{x}$, and using the fact that $\phi(\vec{x})$ is the signed distance to the closest point on the interface,

$$\vec{x}_C = \vec{x} - \phi(\vec{x})\vec{N}, \tag{3.25}$$

can be used to calculate the closest point on the interface where $\vec{N}$ is the local unit normal at $\vec{x}$.

### 3.2. Numerical techniques

A key factor for the success of level set methods is the use of high order high resolution type schemes reviewed in Section 2, for the conservation laws and Hamilton–Jacobi equations. These include in particular the ENO and WENO schemes.

Even with these high order accurate approaches to solving the Hamilton–Jacobi equations, one can obtain surprisingly inaccurate results when the level set function solution becomes too steep or too flat, i.e., discontinuous or poorly conditioned. In [34], Chopp considered an application where certain regions of the flow had level sets piling up on each other increasing the local gradient, and other regions of the flow had level sets that separated from each other flattening out $\phi$. In order to reduce the numerical errors caused by both the steeping and flattening effects, Chopp [34] introduced the notion that one should reinitialize the level set function periodically throughout the calculation. In [156], Rouy and Tourin proposed a numerical method for the shape from shading problem that was later generalized into the modern day reinitialization equation of Sussman et al. [174], using the fact that $|\nabla d| = 1$, for $d$ the signed or unsigned distance to a given set.

Unfortunately, this straightforward reinitialization routine can be slow, especially if it needs to be done every time step although Sussman et al. [174] noted that just a few time iterations are usually needed. In order to obtain reasonable run times, Chopp [34] restricted the calculations of the interface motion and the reinitialization to a small band of points near the $\phi = 0$ isocontour. This idea of computing solutions to

Hamilton–Jacobi equations local to the interface has been studied further in the more recent work of Adalsteinsson and Sethian [1] and Peng et al. [150].

Local methods are important for both solving the Hamilton–Jacobi equation and for reinitializing the level sets so that they do not become discontinuous or poorly conditioned. However, at least in the reinitialization case, it is possible to construct an even faster method that only treats each grid point once while sweeping out from the zero isocontour creating a signed distance function. This algorithm was invented by Tsitsiklis in a pair of papers [181,182]. The most novel part of this algorithm is the extension of Dijkstra's algorithm for computing the taxicab metric to an algorithm for computing Euclidean distance. See for example Sethian [164] and Helmsen et al. [81] for the application of these "fast marching methods" in the level set community.

The great success of level set methods can in part be attributed to the role of curvature in regularizing the level set function such that the proper vanishing viscosity solution is obtained. It is much more difficult to obtain vanishing viscosity solutions with Lagrangian methods that faithfully follow the characteristics. For these methods, one usually has to delete (or add) characteristic information by hand when a shock (or rarefaction) is detected. This ability of level set methods to identify and delete merging characteristics is clearly seen in a purely geometrically driven flow where a square is advected inward normal to itself at constant speed. In the corners of the square, the flow field has merging characteristics that are appropriately deleted by the level set method. On the other hand, repeating the same calculation with a Lagrangian numerical method is difficult since characteristics will merge in the corners of the square but not be automatically deleted. One does not easily obtain the correct viscosity solution. Level set methods are not perfect however, since they tend to incorrectly delete characteristics in under resolved regions of the flow – a behavior frequently called "loss of mass" (or volume) in reference to the error it represents when level sets are used to model incompressible fluid flow. In contrast, despite a lack of explicit enforcement of mass (or volume) conservation, Lagrangian schemes are quite successful in conserving mass since they preserve material characteristics for all time, i.e., characteristics are never deleted.

The difficulty stems from the fact that the level set method cannot accurately tell if characteristics merge, separate, or run parallel in under-resolved regions of the flow. This indeterminacy leads to vanishing viscosity solutions that can incorrectly delete characteristics when they appear to be merging. In [51], Enright et al. designed a hybrid particle level set method to alleviate the mass loss issues associated with level set methods. In the case of fluid flows, knowing a priori that there are no shocks present in the fluid velocity field, one can assert that characteristic information associated with that characteristic field should never be deleted. Particles are randomly seeded near the interface and passively advected with the flow. When marker particles cross over the interface, it indicates that characteristic information has been incorrectly deleted, and these errors are fixed by locally rebuilding the level set function using the characteristic information present in these escaped marker particles.

### 3.3. Fluids and materials

Chronologically, the first attempt to use the level set method for flows involving external physics was in the area of two-phase inviscid compressible flow. Mulder et al. [121] appended the level set equation to the standard equations for one-phase compressible flow. The level set was advected using the velocity of the compressible flow field so that the zero level set of $\phi$ corresponds to particle velocities and can be used to track an interface separating two different compressible fluids. Later, Karni [92] pointed out that such method suffered from spurious oscillations at the interface and proposed a nonconservative fix. A more robust fix was later proposed by Fedkiw et al. [60] by creating a set of fictitious ghost cells on each side of the interface, and populating these ghost cells with a specially chosen ghost fluid that implicitly captures the Rankine–Hugoniot jump conditions across the interface. This method was referred to as the ghost fluid method. Later extensions included the treatment of shocks, detonations, and deflagrations [61], interfaces

separating compressible flows from incompressible flows [18], and interfaces separating Eulerian discretizations of fluids from Lagrangian discretizations of solids [59]. More recently, both Nguyen et al. [125] and Glimm et al. [68] have proposed fully conservative versions of this ghost fluid method. Moreover, the method proposed in [125] is easy to implement in multiple spatial dimensions, works for contacts, shocks, detonations, and deflagrations, and has been shown to prevent the one grid cell per time step spurious wave instabilities (identified by [36]) that occur in stiff under-resolved detonation waves.

The earliest real success in the coupling of the level set method to problems involving external physics came in computing two-phase incompressible flow, in particular see Sussman et al. [174] and Chang et al. [29]. The Navier–Stokes equations were used to model the fluids on both sides of the interface. Generally, the fluids will have different densities and viscosities and the presence of surface tension forces cause the pressure to be discontinuous across the interface as well. Although these early works smeared out these discontinuous quantities across the interface, this was later remedied by Kang et al. [91] using the methods developed by Liu et al. [105]. More recently, Nguyen et al. [124] extended these techniques to treat low speed flames.

A level set regularization procedure was proposed in Harabetian and Osher [75] for ill-posed problems such as vortex motion in incompressible flows. This regularization, coupled with nonoscillatory numerical methods for the resulting level set equations, provides a regularization which is topological and is automatically accomplished through the use of numerical schemes whose viscosity shrinks to zero with grid size. There is no need for explicit filtering, even when singularities appear in the solution. The method also has the advantage of automatically allowing topological changes such as merging of surfaces.

An application of this procedure for incompressible vortex motion was given in Harabetian et al. [76]. An Eulerian, fixed grid, approach to solve the motion of an incompressible fluid, in two and three dimensions, in which the vorticity is concentrated on a lower dimensional set, is provided. The numerical variables for the level sets are actually smooth, thus allowing for accurate numerical simulations. Numerical examples including 2D and 3D vortex sheets, 2D vortex dipole sheets, and point vortices, are given.

Level set type analysis was also used to obtain rigorous results identifying the Wulff minimizing shape and the evolution of growing crystals moving with normal velocity defined as a given positive function of the normal direction, thus verifying a conjecture of Gross. Moreover it was also shown that the Wulff energy decreases monotonically under such an evolution to its minimum [141]. A spinoff came in [151] where it was proven that any 2D Wulff shape can be interpreted as the solution a corresponding Riemann problem for a scalar conservation law – jumps in the direction of the normal correspond to contact discontinuities, smoothly varying thin flat faces correspond to rarefaction curves and planar facets correspond to constant states. The work in [141] also motivated the derivation of a new class of isoperimetric inequalities for convex plane curves [71].

Molecular beam epitaxy (MBE) is a method for growing extremely thin films of material. A new continuum model for the epitaxial growth of thin films has been developed. This new island dynamics model has been designed to capture the larger length scale features. The key idea involves the level-set based motion of islands of various integer levels – see for example [30,74,120].

### *3.4. A variational approach*

In [196] a variational level set approach was developed. Key ideas were the use of a single level set function for each phase, the gradient projection method of [157] to prevent overlap and/or vacuum, and the liberal use of the level set calculus as described earlier. This general variational approach has many applications. The first was to study the behavior of bubbles and droplets in two and three dimensions [197], for example drops falling or remaining attached to a generally irregular ceiling, and mercury sitting on the floor. Many problems in engineering design involve optimizing the geometry to maximize a certain design objective. In [144] the variational level set method was used to analyze a vibrating system whose resonant

frequency or whose spectral gap is to be optimized subject to constraints on the geometry. This variational approach has applications in computer vision as well, e.g., snakes and active contours [26]. This will be discussed further in Section 4.

### 3.5. High codimension motion

Typically level set methods are used to model codimension one objects, e.g., curves in $R^2$ or surfaces in $R^3$. In [16], this technology was extended to treat codimension two objects, e.g., curves in $R^3$, using the intersection of the zero level sets of two functions. This means a curve is determined by

$$\Gamma(t) = \{\vec{x} \,|\, \phi_1(\vec{x}, t) = \phi_2(\vec{x}, t) = 0\}.$$

The geometry of the curve can be derived from $\phi_1$ and $\phi_2$. For example, the tangent to the curve is defined by

$$\vec{T} = \frac{\nabla\phi_1 \times \nabla\phi_2}{|\nabla\phi_1 \times \nabla\phi_2|}.$$

The curvature times the normal is the derivative of the tangent vector along the curve

$$\kappa\vec{N} = \nabla\vec{T} \cdot \vec{T}. \tag{3.26}$$

The normal vectors can be defined by normalizing this quantity

$$\vec{N} = \frac{\kappa\vec{N}}{|\kappa\vec{N}|}. \tag{3.27}$$

The binormal is

$$\vec{B} = \frac{\vec{T} \times \vec{N}}{|\vec{T} \times \vec{N}|}.$$

The torsion times the normal vector is $\tau\vec{N} = -\nabla\vec{B} \cdot \vec{T}$. These geometric quantities are all defined numerically just as in the standard codimension one level set method. Geometric motion of a curve in $R^3$ is thus obtained by solving coupled systems of two evolution equations. This is done locally near $\Gamma(t)$, saving on storage and complexity. See [16] for results involving merging and breaking which appear to agree with the reaction–diffusion limit when appropriate. Another application of this idea comes from the following observation. If we freeze one of the functions, say $\phi_1$, we can generate the motion of curves on a surface. Here the surface is defined by $\{\vec{x} \,|\, \phi_1(\vec{x}) = 0\}$ and the evolving curve is defined by the intersection of that fixed surface with $\{\vec{x} \,|\, \phi_2(\vec{x}, t) = 0\}$. This is useful for path planning on terrain data, see [33].

### 3.6. Geometric optics

In [137] a level-set based approach for ray tracing and for the construction of wavefronts in geometric optics was introduced. The approach automatically handles the multi-valued solutions that appear and automatically resolves the wavefronts. The key idea, first introduced in [50] in a "segment projection" (rather than a level set) approach, is to use the linear Liouville equation in twice as many independent variables and solve in this higher dimensional space via the idea introduced in [16]. In 2D ray tracing, this involves solving for an evolving curve in $x, y, \theta$ space, where $\theta$ is the angle of the normal to the curve. This uses two level set functions and gives codimension 2 motion in 3 space dimension plus time. A local level set method can be used to make the complexity tractable – $O(n^2 \log(n))$ – for $n$ the number of points on the

curve for every time iteration. The memory requirement is $O(n^2)$. In 3D ray tracing, this involves solving for an evolving 2D surface in $x, y, z, \theta, \psi$ space, where $\theta$ and $\psi$ give the angle of the normal, and results in codimension 3 motion in 5 space dimension plus time. The complexity goes up by a power of $n$ over the 2D case, as does the memory requirement. Again, this involves a local level set method, this time using three level set functions. The interested reader is referred to [159,172] for a different Eulerian approach.

### 3.7. Computing discontinuous solutions to Hamilton–Jacobi equations

Hamilton–Jacobi equations of the form

$$\phi_t + H(\vec{x}, t, \phi, \nabla\phi) = 0 \tag{3.28}$$

have uniformly continuous solutions if $H$ is nondecreasing in $\phi$. However, there are interesting cases in which this hypothesis fails. Moreover, discontinuous initial data are appropriate for some problems in control theory and differential games. The solution devised in [67] uses the evolution of the level set of an auxiliary level set equation. The idea has antecedents in [133] where it was proven that, under reasonable circumstances, the zero level set of the viscosity solution of

$$\phi_t + H(\vec{x}, \nabla\phi) = 0$$

for $H$ homogeneous of degree one in $\nabla\phi$ is the same as the $t$ level set of the viscosity solution of

$$H(\vec{x}, \nabla\psi) = 1,$$

i.e.,

$$\{\vec{x} \,|\, \phi(\vec{x}, t) = 0\} = \{\vec{x} \,|\, \psi(\vec{x}) = t\}. \tag{3.29}$$

This idea was used in [67] to go one dimension higher in Eq. (3.28). This leads to new and successful numerical methods for a wide class of initial value problems for Hamilton–Jacobi equations with discontinuous solutions, see [180].

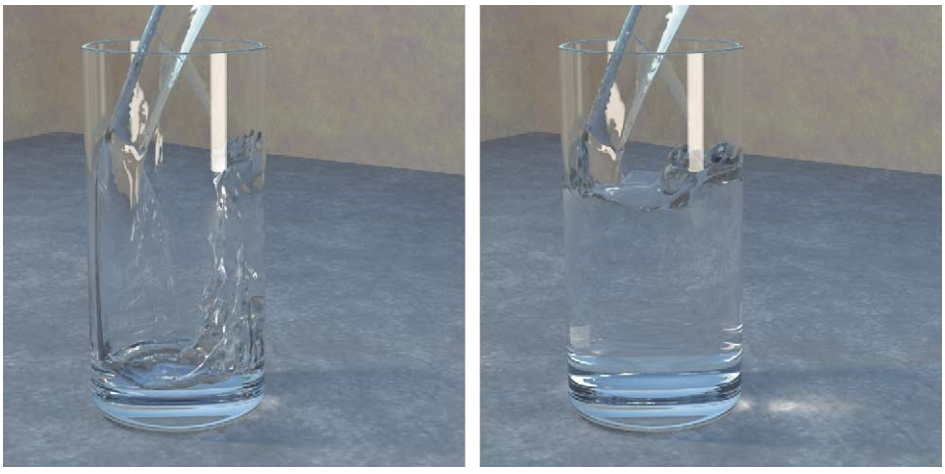

Fig. 1. The level set method can be used to create impressively smooth surfaces on relatively coarse grids. Here the particle level set method from [51] was used to represent the interface separating water from air as water is being poured into a glass. For more details, see [52].

### 3.8. Additional topics

Level set methods have been applied to a variety of other problems as well. They have been used to compute solutions to Stefan problems to study crystal growth [31,95], to simulate water and fire for computer graphics applications [52,64,123], and to reconstruct 3D models from arbitrary unorganized data points [198,199]. Fig. 1 shows an example calculation of water being poured into a glass. Here the level set method gives a smooth visually realistic appearance to the water surface. Moreover this calculation can be carried out using a reasonable number of grid cells and without the need for complicated surgical methods to treat interface pinching and merging. Fig. 2 shows an example calculation of a sphere catching on fire. Here the level set method allows one to accurately represent the thin flame zone that separates the unreacted gaseous fuel from the reacted hot gaseous products. Gaseous expansion can then be accurately modeled across this interfacial zone. Fig. 3 (left) shows an unorganized data point set extracted from an

Fig. 2. The level set method allows one to accurately represent the thin flame zone that separates the unreacted gaseous fuel from the reacted hot gaseous products. This allows one to more accurately model the gaseous expansion across this interfacial zone. Here the level set method is used to simulate a ball catching on fire. For more details, see [123] where these calculations were carried out using methods first proposed in [124].

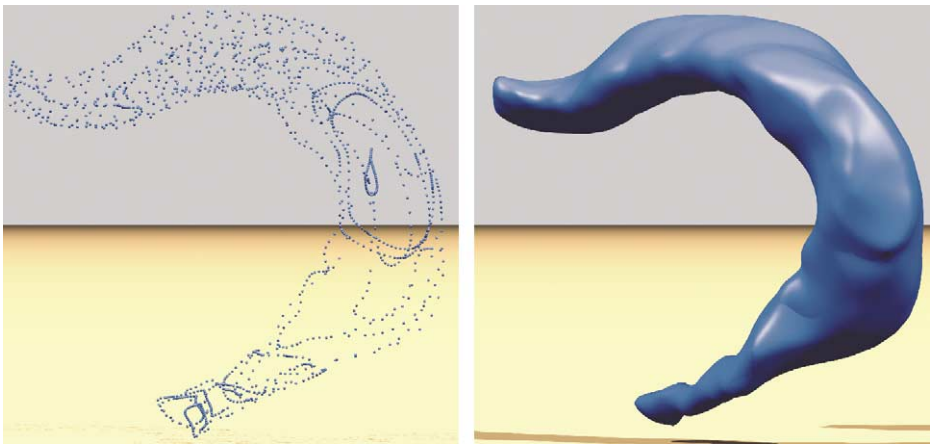

Fig. 3. The figure on the left shows an unorganized data point set extracted from an MRI of a rat brain, while the figure on the right shows a level set reconstruction of the rat brain using only these data points. Note how well the level set method can accurately predict connectivity. For more details, see [198].

MRI of a rat brain, while Fig. 3 (right) shows a level set reconstruction of the rat brain using only these data points. Note how well the level set method can accurately predict connectivity. The use of level set methods for computer vision will be discussed further in Section 4.

## 4. Image processing and computer vision

The use of partial differential equations (PDEs) and curvature driven flows in image processing and computer vision has become an active research topic in the past few years. The basic idea is to deform a given curve, surface, or image with a PDE, and obtain the desired result as the solution of this PDE. Sometimes, as in the case of color images, a system of coupled PDEs is used. The art behind this technique is in the design, analysis, and numerical implementation of these PDEs.

Partial differential equations can be obtained from variational problems. Assume a variational approach to an image processing problem formulated as a minimization of $\mathscr{U}(u)$, where $\mathscr{U}$ is a given energy computed over the image (or surface) $u$. Let $\mathscr{F}(\cdot)$ denote the Euler derivative (first variation) of $\mathscr{U}$. Since under general assumptions, a necessary condition for $u$ to be a minimizer of $\mathscr{U}$ is that $\mathscr{F}(u) = 0$, the (local) minima may be computed via the steady state solution of the equation

$$\frac{\partial u}{\partial t} = -\mathscr{F}(u),$$

where $t$ is an "artificial" time marching parameter. PDEs obtained in this way have been used already for quite some time in computer vision and image processing, and the literature is large. The most classical example is the Dirichlet integral

$$\mathscr{U}(u) = \int |\nabla u|^2(x)\mathrm{d}x,$$

which is associated with the linear heat equation

$$\frac{\partial u}{\partial t}(x,t) = \Delta u(x).$$

Extensive research is also being done on the direct derivation of evolution equations which are not necessarily obtained from the energy approaches. The attributes of PDEs in image processing are discussed for example in [22,161]. In the pioneering paper [2] the authors prove that a few basic image processing principles naturally lead to PDEs.

Note that when considering PDEs for image processing and numerical implementations, we are dealing with derivatives of nonsmooth signals, and the right framework must be defined. As introduced by the image processing group formerly at CEREMADE [2,3], the theory of *viscosity solutions* provides a framework for rigorously employing a partial differential formalism, in spite of the fact that the image may not be smooth enough to give a classical definition to the derivatives involved in the PDE. These works also showed with a very elegant axiomatic approach the importance of PDEs in image processing.

Ideas on the use of PDEs in image processing go back at least to Gabor [66] and to Jain [87]. The field took off thanks to the independent works of Koenderink [99] and Witkin [191]. These researchers rigorously introduced the notion of *scale-space*, i.e., the representation of images simultaneously at multiple scales. In their work, the multi-scale image representation is obtained by Gaussian filtering, see below. This is equivalent to deforming the original image via the classical heat equation, obtaining in this way an isotropic diffusion flow. In the late 1980s, Hummel [84] noted that the heat flow is not the only parabolic PDE that can be used to create a scale-space, and indeed argued that an evolution equation which satisfies the

maximum principle will define a scale-space as well. The maximum principle appears to be a natural mathematical translation of *causality*. Koenderink once again made a major contribution into the PDEs arena when he suggested to add a thresholding operation to the process of Gaussian filtering. As later suggested by Merriman et al. [118,119] and by Ruuth et al. [158], and proved by a number of groups [8,53,85,86], this leads to a curvature motion geometric PDE, one of the most famous among geometric PDEs. In [160], Ruuth et al. extended it to diffusion generated motion of curves in $\mathbb{R}^3$. Solving a vector heat equation and thresholding lead to moving the curve in the direction of the normal with velocity equal to its curvature.

Perona and Malik's work [152] on anisotropic diffusion, together with the work by Rudin et al. on total variation [157] and by Osher and Rudin on shock filters [142], have been among the most influential papers in the area, explicitly showing the importance of understanding nonlinear PDEs theory to deal with images. They proposed to replace the linear Gaussian smoothing, equivalent to isotropic diffusion via the heat flow, by a selective nonlinear diffusion that preserves edges, see below. Their work opened a number of theoretical and practical questions that continue to occupy the PDEs image processing community, see e.g. [3,155]. We should also point out that, at about the same time, Price et al. published a very interesting paper on the use of Turing's reaction–diffusion theory for a number of image processing problems [154]. Reaction diffusion equations were also suggested to create artificial texture [184,193].

Many of the PDEs used in image processing and computer vision are based on moving curves and surfaces with curvature based velocities. In this area, the level-set numerical method developed by Osher and Sethian [145], which is reviewed in Section 3, is very influential and examples will be provided later in this section. The representation of static objects as level sets (zero-sets) is of course not completely new to the computer vision and image processing communities, since it is one of the fundamental techniques in mathematical morphology [162]. Considering the image itself as a collection of its level sets, and not just as the level set of a higher dimensional function, is a key concept in the PDEs community [2]. Implicit surfaces and level set representations appear in computer graphics as well [12,192].

Other works, like the segmentation approach of Mumford and Shah [122] and the snakes of Kass et al. [93] have been very influential in the PDEs community as well. More on this will be mentioned below.

It should be noted that a number of the above approaches rely quite heavily on a large number of mathematical advances in differential geometry for curve evolution [70] and in viscosity solutions theory for curvature motion (see e.g. [32,54]).

One of the basic ideas behind this area is that the fact that images are represented in digital computers in the form of discrete objects should not limit the tools to those of discrete mathematics. It is "legal" to use tools from differential equations and differential geometry, and then deal with the computer implementation of the algorithms from the point of view of numerical analysis. The result of this approach is then not only a set of state of the art image processing techniques, but more a new complementary approach to classical techniques.

The frameworks of PDEs and geometry driven diffusion have been applied to many problems in image processing and computer vision, since the seminal works mentioned above. Examples include continuous mathematical morphology, invariant shape analysis, shape from shading, segmentation, tracking, object detection, optical flow, stereo, image denoising, image sharpening, contrast enhancement, and image quantization. In this section we provide a few examples of these. Since this is a paper in honor of Osher, the presentation of the examples is of course biased by his involvement and contributions in the area. Important sources of literature in the area are the excellent collection of papers in the book edited by Romeny [155], the book by Guichard and Morel [72] that contains an outstanding description of the topic from the point of view of iterated infinitesimal filters, Sethian's book on level sets [163], the book of Osher and Fedkiw [139], Lindeberg's book which is a classic in scale-space theory [104], Weickert's book on anisotropic diffusion in image processing [188], Kimmel's lecture notes [97], Sapiro's recent book [161], Toga's book on brain warping that includes a number of PDEs based algorithms [178], and the special March 1998

issue of the IEEE Transactions on Image Processing [22]. The interested reader will find in these publications some fascinating contributions in the area of PDEs in image processing and computer vision, much beyond the few introductory examples provided below.

### 4.1. The total variation model for image denoising

As mentioned above, the use of PDEs for image enhancement has become one of the most active research areas in image processing [22]. In particular, diffusion equations are commonly used for image regularization, denoising, and multi-scale representations (representing the image simultaneously at several scales or levels of resolution). This started with the pioneering works in [99,191], where the authors suggested the use of the linear heat flow for this task, given by

$$\frac{\partial u}{\partial t} = \Delta u, \tag{4.1}$$

where $u : \Omega \subset \mathbb{R}^2 \to \mathbb{R}$ represents the image gray values (the original noisy image is used as initial condition). As it is well known, this equation is the gradient-descent of

$$\int_\Omega \|\nabla u\|^2 \mathrm{d}\Omega. \tag{4.2}$$

An example of the effect of the linear heat flow or Laplace Eq. (4.1) is presented in Fig. 4 (the numerical implementation is based on [157]). It is clear that although this technique can be used to denoise images, it is also blurring them. That is, not only the noise is being removed, but the edges and the relevant information is getting destroyed as well. Moreover, it can be shown that edges are destroyed faster than the actual noise is removed [11]. The effect of this is that if for example this is used as a pre-process for image segmentation (see Fig. 4), then the exact location of the objects in the image is modified. There is then a need to remove the noise, and to simplify the image, without disturbing the main objects in it. The approaches now described address this issue.

Two directions were taken to address this problem. On one hand, Perona and Malik [152] suggested to replace the linear heat flow by a PDE that preserves edges. Simultaneously, Rudin et al. [157] started to look at the modification of the variational problem (4.2). In certain cases, the two directions can be shown to be equivalent, the PDE being the gradient descent of the proposed variational formulation. Rudin et al. suggested to replace the linear $L_2$ norm in (4.2) by the edge oriented Total Variation (TV) norm in the energy, thereby obtaining

$$\int_\Omega \|\nabla u\| \mathrm{d}\Omega, \tag{4.3}$$

Fig. 4. Example of the heat flow (isotropic diffusion). On the left we have the original image and on the middle two different time steps of the diffusion flow, showing how the image is getting blurred. This blurring impedes the achievement of an accurate segmentation, right figure. See below for details on the segmentation technique.

Fig. 5. Example of the TV flow for anisotropic diffusion. On the left we have the original image and on the middle the result of the flow, showing how the edges are much better preserved than with the isotropic flow. This allows, for example, to perform accurate segmentation, as shown on the right (compare to previous figure). See below for details on the segmentation technique.

whose gradient descent flow is given by

$$\frac{\partial u}{\partial t} = \operatorname{div}\left(\frac{\nabla u}{\|\nabla u\|}\right). \tag{4.4}$$

We notice that in comparison with the linear heat flow, the TV one has a stopping term of the form $1/\|\nabla u\|$. This helps to preserve edges, as can be seen in Fig. 5 (see [157] for details on the numerical implementation of this equation). Rudin et al. also suggested to add constraints to this minimization, in order to avoid reaching the trivial (flat) steady state, thereby improving the results in Fig. 5. In this case the corresponding Lagrange multiplier is evaluated via a projection method that was found to be useful in other applications as well, e.g. [144].

From the point of view of edge preservation, the TV flow is optimal if we limit ourselves to convex functionals [11]. Motivated by the seminal work of Perona and Malik [152] and that of Rudin et al. [157], significant theoretical and practical studies have been conducted in this kind of anisotropic diffusion flows in general and the TV flow in particular. Numerical implementation issues have been studied in, e.g. [25,188,116]. Formal mathematical properties have been studied in, e.g., [3,188], and more recently in [4,5] with a full study of the TV flow in general dimensions. This work has also in part motivated researchers to connect wavelets with the TV space, e.g. [35].

To conclude, let us note that the TV model is frequently used as a regularization term for inverse problems. In Fig. 6, obtained from the work of Chan and Wong [28], we see an example. Full details on this equation and how the figures have been obtained can be found in [28].

### *4.2. Images on implicit surfaces*

In the last subsection we dealt with images on the plane. There is of course more than that in practice, as data can be defined on surfaces. In [10] the authors dealt with this issue. A framework for solving variational problems and partial differential equations for scalar and vector-valued data defined on surfaces was introduced. The key idea is to implicitly represent the static surface as the level set of a higher dimensional static function, and solve the surface equations in a fixed Cartesian coordinate system using this new embedding function. This leads to the use of simple and well-studied numerical techniques instead of complicated (and not always mathematically justified) implementations. Typically, the software with the implicit approach described below has only a few lines of code, in contrast with packages based on triangulated surfaces that lead to hundreds, if not thousands, of lines.

Implicit surfaces can be obtained for example from the algorithms in [44,65,176,182,199]. Applications of PDEs on surfaces include computer graphics [183,184,193], visualization [40], weathering simulation [41],

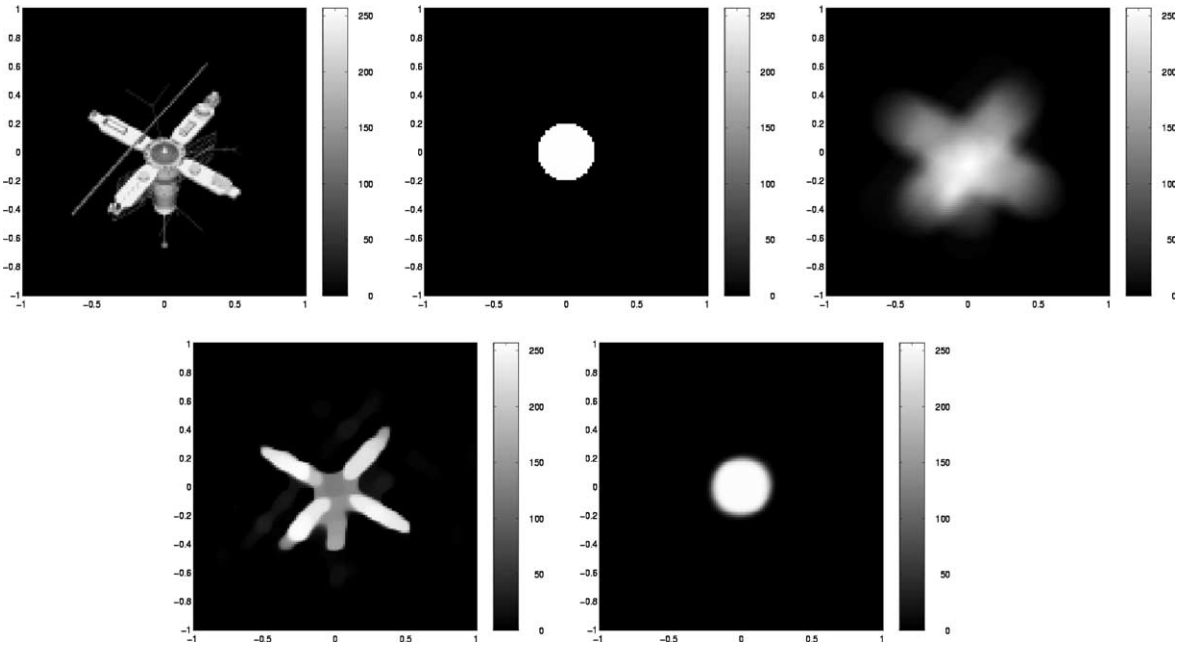

Fig. 6. Example of the use of the TV model as a regularization term for inverse problems. The first row shows from left to right the original image, the out-of-focus blur, and the blurred image. The basic idea is to recover the original image, without knowing the blurring function, from the blurred data. This problem is known as blind deconvolution. The recovered image and blurring function are shown on the second row. The technique developed by Chan and Wong uses the TV model of Rudin–Osher–Fatemi for this problem.

vector field computation or interpolation process [153,190], inverse problems [58], and surface parameterization [43].

We assume then that the 3D surface $\mathscr{S}$ of interest is given in implicit form, as the zero level set of a given function $\phi : \mathbb{R}^3 \to \mathbb{R}$. This function is negative inside the closed bounded region defined by $\mathscr{S}$, positive outside, Lipschitz continuous a.e., with $\mathscr{S} \equiv \{x \in \mathbb{R}^3 : \phi(x) = 0\}$. To ensure that the data, which needs not to be defined outside of the surface originally, is now defined in the whole band, one simple possibility is to extend this data $u$ defined on $\mathscr{S}$ (i.e., the zero level set of $\phi$) in such a form that it is constant normal to each level set of $\phi$. This, which is easily realizable [31], is only done if the data is not already defined in the whole embedding space.

We will exemplify the framework with the simplest case, the heat flow or Laplace equation for scalar data defined on a surface. For scalar data $u$ defined on the plane, i.e., $u(x,y) : \Omega \subset \mathbb{R}^2 \to \mathbb{R}$, as we saw before, the heat flow is given by (4.1), and its corresponding energy by (4.2). If we now want to smooth scalar data $u$ defined on a surface $\mathscr{S}$, i.e., $u(x,y) : \mathscr{S} \to \mathbb{R}$, we must find the minimizer of the energy given by

$$\frac{1}{2}\int_{\mathscr{S}} \|\nabla_{\mathscr{S}} u\|^2 \mathrm{d}\mathscr{S}. \tag{4.5}$$

The equation that minimizes this energy is its gradient descent flow (e.g. [173])

$$\frac{\partial u}{\partial t} = \Delta_{\mathscr{S}} u. \tag{4.6}$$

Here $\nabla_{\mathscr{S}}$ is the intrinsic gradient and $\Delta_{\mathscr{S}}$ the intrinsic Laplacian or Laplace–Beltrami operator.

Classically, Eq. (4.6) would be implemented in a triangulated surface, giving place to sophisticated and elaborated algorithms even for such simple flows. We now show how to simplify this when considering implicit representations.

Let $\vec{v}$ be a generic 3D vector, and $P_{\vec{v}}$ the operator that projects a given 3D vector onto the plane orthogonal to $\vec{v}$. It is then easy to show that the harmonic energy (4.5) [45] is equivalent to (see for example [171])

$$\frac{1}{2}\int_{\mathscr{S}} \|P_{\vec{N}}\nabla u\|^2 \mathrm{d}\mathscr{S}, \tag{4.7}$$

where $\vec{N}$ is the normal to the surface $\mathscr{S}$. In other words, $\nabla_{\mathscr{S}} u = P_{\vec{N}}\nabla u$. That is, the gradient intrinsic to the surface ($\nabla_{\mathscr{S}}$) is just the projection onto the surface of the 3D Cartesian (classical) gradient $\nabla$. We now embed this in the function $\phi$:

$$\frac{1}{2}\int_{\mathscr{S}} \|\nabla_{\mathscr{S}} u\|^2 \mathrm{d}\mathscr{S} = \frac{1}{2}\int_{\Omega\in\mathbb{R}^3} \|P_{\nabla\phi}\nabla u\|^2 \delta(\phi)\|\nabla\phi\| \mathrm{d}x,$$

where $\delta(\cdot)$ stands for the delta of Dirac, and all the expressions above are considered in the sense of distributions. Note that first we got rid of intrinsic derivatives by replacing $\nabla_{\mathscr{S}}$ by $P_{\vec{N}}\nabla u$ (or $P_{\nabla\phi}\nabla u$) and then replaced the intrinsic integration ($\int_{\mathscr{S}} \mathrm{d}\mathscr{S}$) by the explicit one ($\int_{\Omega\in\mathbb{R}^3} \mathrm{d}x$) using the delta function. Intuitively, although the energy lives in the full space, the delta function forces the penalty to be effective only on the level set of interest. The gradient descent of this energy is given by

$$\frac{\partial u}{\partial t} = \nabla\cdot(P_{\nabla\phi}\nabla u). \tag{4.8}$$

In other words, this equation corresponds to the intrinsic heat flow for data on an implicit surface. But all the gradients in this PDE are defined in the 3D Cartesian space, not in the surface $\mathscr{S}$ (this is why we need the data to be defined at least on a band around the surface). The numerical implementation is then straightforward. Once again, due to the implicit representation, classic numerics are used, avoiding elaborate projections onto discrete surfaces and discretization on general meshes, e.g. [83]. The same framework can be applied to other variational formulations as well as to PDEs defined on surfaces, e.g., the ones exemplified below [10]. In addition, it can be applied to the TV model described above for images on the plane. An example of this is presented in Fig. 7. These figures were reproduced from [10], where full numerical details are given.

A particularly interesting example is obtained when we have unit vectors defined on the surface. That is, we have data of the form $u : \mathscr{S} \to S^{n-1}$. When $n = 3$ our unit vectors lie on the sphere. Following the work [175] for color images defined on the plane, we show in Fig. 8 how to denoise a color image painted on an implicit surface. The basic idea is to normalize the RGB vector (a 3D vector) to a unit vector representing the chroma, and diffuse this unit vector with the harmonic maps flow embedded on the implicit surface extending the intrinsic heat flow example presented above. The corresponding magnitude, representing the brightness, is smoothed separately via scalar diffusion flows as those presented before for images on the plane (e.g., an intrinsic TV anisotropic heat flow). That is, we have to regularize a map from the zero level set onto $S^2$ (the chroma) and another one onto $\mathbb{R}$ (the brightness). Details on the use of harmonic maps equations for this color denoising flow can be found in [175], while [10] gives a full description of the corresponding intrinsic flow for 3D implicit surface, as it was used to generate Fig. 8. Note that the basic numerical implementation of these equations, both on the plane [175] and on 3D implicit surfaces [10], are connected to the techniques presented in [157] to implement the TV flow.

Following the same framework and the work in [183,184,193], we show in Fig. 9 the result of reaction diffusion flows solved on implicit surfaces in order to generate intrinsic patterns. Once again, the precise equations are given in [10].

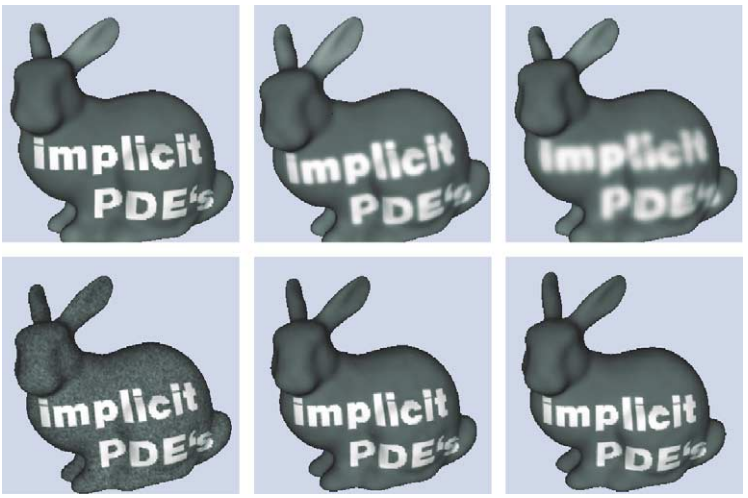


Fig. 7. Intrinsic heat flow (first row, original, and 15 and 50 iterations, respectively) and TV flow (second row, original, and 50 and 90 iterations, respectively) for data defined on surfaces. Note how as expected, the heat flow blurs the data while the TV flow removes the noise while preserving the sharp edges (constraints on the noise have been added to the flow).

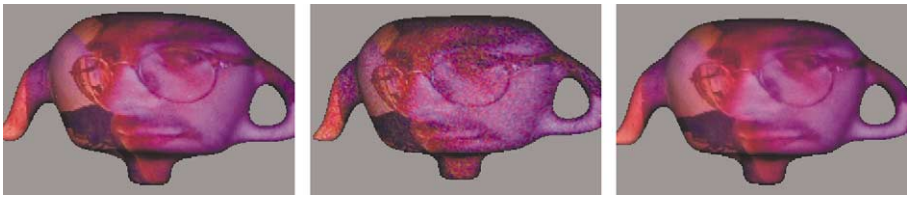

Fig. 8. Intrinsic vector field regularization. Left: original color image. Middle: heavy noise has been added to the three color channels. Right: color image reconstructed after 20 steps of anisotropic diffusion of the chroma vectors.

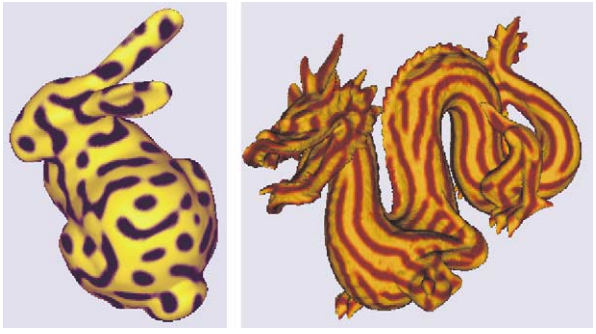

Fig. 9. Texture synthesis via intrinsic reaction–diffusion flows on implicit surfaces. Left: isotropic. Right: anisotropic.

Finally, inspired by the work on line integral convolution [17] and that on anisotropic diffusion [152], the authors of [40] suggested to use anisotropic diffusion to visualize flows in 2D and 3D. The basic idea is, starting from a random image, anisotropically diffuse it in the directions dictated by the flow field. The

authors presented very nice results both in 2D (flows on the plane) and 3D (flows on a surface), but once again using triangulated surfaces which introduce many computational difficulties. In a straightforward fashion we can compute these anisotropic diffusion equations on implicit surfaces with the framework from [10] that we have just described, and some results are presented in Fig. 10. See [10] for the exact visualization equations and their numerical implementation.

### 4.3. The level set method in image processing and computer vision

We now present a number of examples on the use of the Osher–Sethian level set method reviewed in Section 3 for problems in image processing and computer vision, in particular for image segmentation.

One of the most popular applications of level set methods in image processing and computer vision is for image segmentation. The contributions in this area started shortly after the work in [96] (which is one of the first papers in computer vision using the level set method) by the works in [19,114,115]. These authors showed how to embed in the level set framework the pioneering work on snakes and active contours by Kass et al. [93].

Consider the image on the left of Fig. 11. Kass et al. suggested to detect the objects in this image (segment the image) starting with a curve that surrounds the object/s, and letting the curve deform (active-contour/snake) toward the boundary of the objects. The deformation is driven by the minimization of a

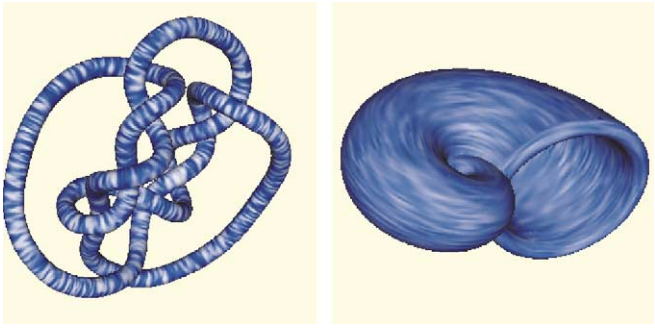

Fig. 10. Flow visualization on implicit 3D surfaces via intrinsic anisotropic diffusion flows. Left: flow aligned with the major principal direction of the surface. Right: flow aligned with the minor principal direction of the surface. Pseudo-color representation of scalar data is used.

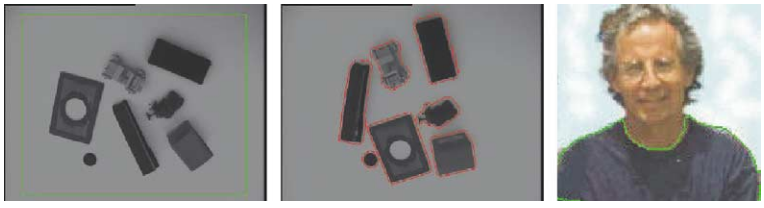

Fig. 11. Level-set based object segmentation. The first figure on the left shows the original image and original contour, surrounding an unknown number of objects. The results of the geodesic active contours is given in the middle image (see the mentioned work of Caselles–Kimmel–Sapiro for details on the numerical implementation of this geodesic flow). The properties of using the level set framework are clear in this example. It not only allows for very accurate computations of geometric characteristics such as curvature but also freely permits topological changes, thereby detecting all of the unknown number of objects. The image in the right is a result of the geodesic active contours framework implemented following Cohen and Kimmel.

given energy that penalizes nonsmooth curves that do not sit at the objects boundaries. The authors of [93] proposed a Lagrangian implementation of the curve deformation process, while Caselles et al. [21] and Malladi et al. [114] pioneered the use of the level set method for this approach. This added the classical topological freedom, thereby allowing the detection of multiple objects without prior knowledge of their number. Later McInerney and Terzopoulos showed a technique based on Lagrangian implementation to achieve this [117]. Following this work, in [20] (see also [21,94,149,165,177,189] for pioneering extensions of this to object tracking), the authors showed that both approaches can be formally unified if one considers an energy given by

$$E(\mathscr{C}) = \int_{\mathscr{C}} g(\mathscr{C})\,\mathrm{d}s, \tag{4.9}$$

where $\mathrm{d}s$ is the Euclidean arc-length over the deforming curve $\mathscr{C} : [a, b] \to \mathbb{R}^2$ and $g(\cdot)$ is a function that penalizes curves that do not sit on the objects boundaries (a function of the image gradient for example). That is, image segmentation has been translated into finding a curve minimizing (4.9), thereby a geodesic in a space with metric $g(\cdot)$. The geodesic was computed using the level set method. Examples are provided in Fig. 11.

When describing image segmentation, variational problems, and PDEs, we can not avoid but think about the famous Mumford–Shah contribution [122], and ask ourselves the relationship between these techniques. Some of this relationship is described in [161], while additional one comes to light from recent works connecting the Mumford–Shah model and level set techniques, see for example the results by Paragios and Deriche [149], by Yezzi and Soatto [194], and by Chan and Vese [27,187]. One of the ideas in this direction is presented in [27,187], which is inspired in part by Zhao et al. [196]. In [27,187], multiple phases and their boundaries, represented via the level set method, evolve and interact in time, to minimize a bulk-surface energy. Combining several level set functions together, triple junctions were also represented and evolved in time. Based on these ideas, Chan and Vese presented a multi-phase level set model for image segmentation. Triple junctions and complex topologies are segmented using more than one level set function. An example is provided in Fig. 12, while details are given in their paper. In this example, a multi-phase model with four phases is used, obtained by combining two level set functions. Here, the phases and their boundaries evolve in time, by minimizing an energy related to the Mumford–Shah piecewise-constant model for segmentation. We show the evolution of the curves and of the four phases, in a level set framework.

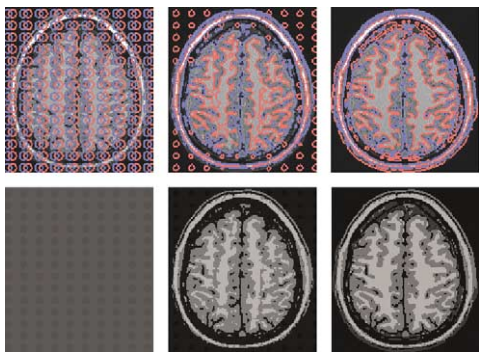

Fig. 12. Evolution of the four-phase segmentation model from [27], using two level set functions: evolving curves (top) and phases (bottom). The fundamental use of the level set implementation is once again observed here, since the splitting and merging of the evolving curves is automatically handled, with no programming effort.

### 4.4. Shape from shading

According to the so called *Lambertian* shading rule, the 2D array of pixel gray levels, corresponding to the shading of a 3D object, is proportional to the cosine of the angle between the light source direction and the surface normal. The shape from shading problem is the inverse problem of reconstructing the 3D surface from this shading data. The history of this problem is extensive. Here we describe a basic technique, developed by Kimmel and Bruckstein [98] to address this problem. We remark that this work by Kimmel and Bruckstein on shape from shading using curve evolution and level sets is inspired in part by the work of Osher in [133]. This presents the general connection between the unsteady and steady approaches to curve and surface evolution. An outstanding contribution to the problem was done in [156], based on the theory of viscosity solutions, see also [126]. More details and an extensive literature can be found in these references.

Consider a smooth surface, actually a graph, given by $z(x,y)$. According to the Lambertian shading rule, the shading image $I(x,y)$ is equal (or proportional) to the inner product between the light direction $\hat{l} = (0,0,1)$ and the normal $\vec{\mathcal{N}}(x,y)$ to the parameterized surface. This gives the so called *irradiance equation*

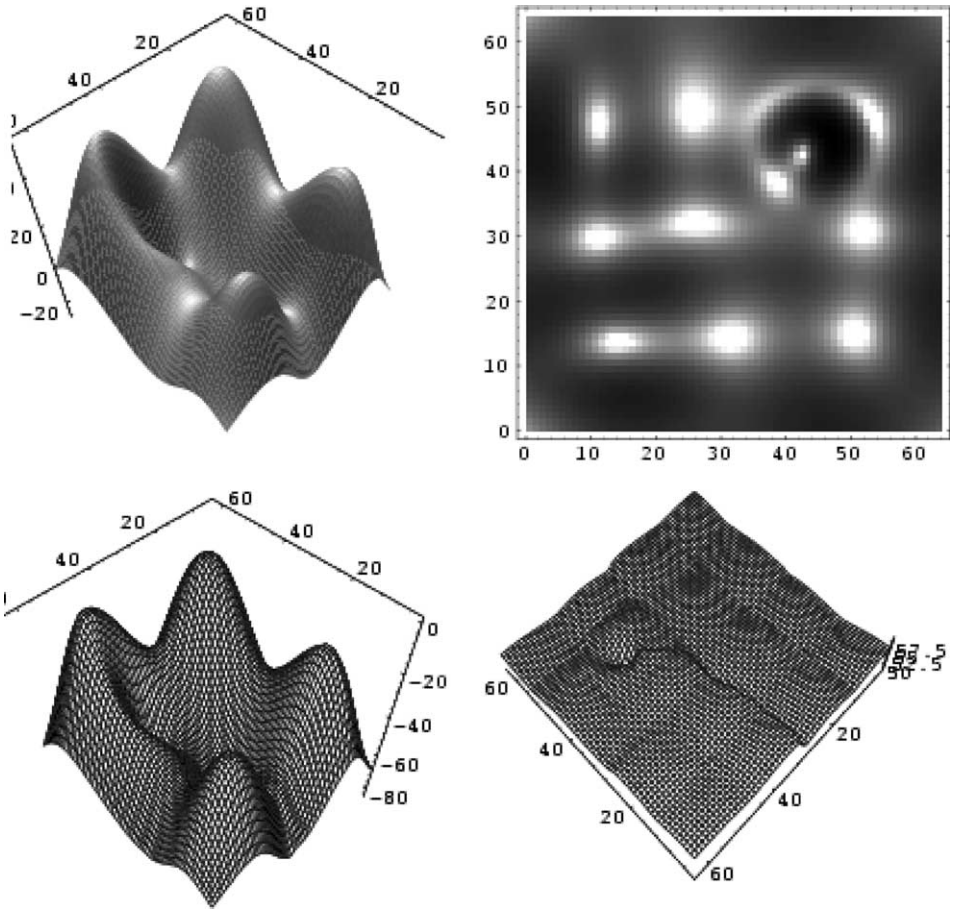


Fig. 13. Example of shape from shading via curve evolution. The figure shows the original surface, the simulated shading, the reconstructed surface, and the reconstruction error.

$$I(x,y) = \hat{l} \cdot \vec{\mathcal{N}} = \frac{1}{\sqrt{1+p^2+q^2}},$$

where $p := \partial z/\partial x$ and $q := \partial z/\partial y$. Starting from a small circle around a singular point, Bruckstein [15] observed that equal height contours $\mathscr{C}(p,t) : S \to \mathbb{R}^2$ of the surface $z$ ($t$ stands for the height) hold

$$\frac{\partial \mathscr{C}}{\partial t} = \frac{I}{\sqrt{1-I^2}}\vec{n},$$

where now $\vec{n}$ is the 2D unit normal to the equal height contour (or level set of $z$). This means that the classical shape from shading problem is simply a curve evolution problem, and as so, we can use all the curve evolution machinery to solve it. In particular, we can use both the level set and the fast marching numerical techniques (the weight for the distance is always positive and given by $\sqrt{1/I^2-1}$). An example, courtesy of the authors of [98], is presented in Fig. 13. This shows another example of how, without being directly involved in this, Osher's work in numerical analysis has influenced a classical problem in computer vision.

## 5. Concluding remarks

In this paper, we have reviewed some of the major contributions of Stanley Osher to the broad area of scientific computation. It is clear from the works we have reviewed, and from the references to his papers in the literature, that Osher's contributions are not limited to the areas where he is directly involved. An example of this is image segmentation, where his work with colleagues on level set and multi-phase motion has been crucial for others to produce state-of-the-art results. The simulation of natural phenomena in computer graphics is yet another example of how people are using his contributions in a completely different area. Another more recent example is his contribution, shared with Harten and other colleagues, on ENO and its derivations, currently being used in wavelets and approximation theory, without Osher being directly involved in that line of research. The fact that his research has reached such diverse disciplines is truly remarkable. Some of Osher's characteristics and contributions are not written in any of his papers. Still at 60, he is full of ideas and energy, and has a fundamental characteristic for doing good research: He considers science fun! (let us not forget that his last name comes from the Hebrew word "happiness"). We are looking forward to seeing Osher's contributions in the next 60 years, though most probably somebody else will have to write the review.

## References

[1] D. Adalsteinsson, J. Sethian, A fast level set method for propagating interfaces, J. Comput. Phys. 118 (1995) 269–277.
[2] L. Alvarez, F. Guichard, P.L. Lions, J.M. Morel, Axioms and fundamental equations of image processing, Arch. Rational Mech. 123 (1993) 199–257.
[3] L. Alvarez, P.L. Lions, J.M. Morel, Image selective smoothing and edge detection by nonlinear diffusion, SIAM J. Numer. Anal. 29 (1992) 845–866.
[4] F. Andreu, C. Ballester, V. Caselles, J.M. Mazon, The Dirichlet problem for the total variation flow, J. Funct. Anal. 180 (2001) 347–403.
[5] F. Andreu, C. Ballester, V. Caselles, J.M. Mazon, Minimizing total variation flow, Differential Integral Equations 14 (2001) 321–360.
[6] D. Balsara, C.-W. Shu, Monotonicity preserving weighted essentially non-oscillatory schemes with increasingly high order of accuracy, J. Comput. Phys. 160 (2000) 405–452.
[7] M. Bardi, S. Osher, The nonconvex multi-dimensional Riemann problem for Hamilton–Jacobi equations, SIAM J. Numer. Anal. 22 (1991) 344–351.

[8] G. Barles, C. Georgelin, A simple proof of convergence for an approximation scheme for computing motions by mean curvature, SIAM J. Numer. Anal. 32 (1995) 484–500.
[9] M. Berger, A. Colella, Local adaptive mesh refinement for shock hydrodynamics, J. Comput. Phys. 82 (1989) 64–84.
[10] M. Bertalmio, L.T. Cheng, S. Osher, G. Sapiro, Variational problems and partial differential equations on implicit surfaces, J. Comput. Phys. 174 (2001) 759–780.
[11] M. Black, G. Sapiro, D. Marimont, D. Heeger, Robust anisotropic diffusion, IEEE Trans. Image Process. 7 (3) (1998) 421–432.
[12] J. Bloomenthal, Introduction to Implicit Surfaces, Morgan Kaufmann, San Francisco, California, 1997.
[13] J.P. Boris, D.L. Book, Flux corrected transport I, SHASTA, a fluid transport algorithm that works, J. Comput. Phys. 11 (1973) 38–69.
[14] Y. Brenier, S. Osher, The discrete one-sided Lipschitz condition for convex scalar conservation laws, SIAM J. Numer. Anal. 25 (1988) 8–23.
[15] A.M. Bruckstein, On shape from shading, Comput. Vision Graph. Image Process. 44 (1988) 139–154.
[16] P. Burchard, L.-T. Cheng, B. Merriman, S. Osher, Motion of curves in three spatial dimensions using a level set approach, J. Comput. Phys. 165 (2001) 463–502.
[17] B. Cabral, C. Leedom, Imaging vector fields using line integral convolution, ACM Comput. Graph. (SIGGRAPH '93) 27 (4) (1993) 263–272.
[18] R. Caiden, R. Fedkiw, C. Anderson, A numerical method for two-phase flow consisting of separate compressible and incompressible regions, J. Comput. Phys. 166 (2001) 1–27.
[19] V. Caselles, F. Catte, T. Coll, F. Dibos, A geometric model for active contours, Numer. Math. 66 (1993) 1–31.
[20] V. Caselles, R. Kimmel, G. Sapiro, Geodesic active contours, Int. J. Comput. Vision 22 (1) (1997) 61–79.
[21] V. Caselles, R. Kimmel, G. Sapiro, C. Sbert, Minimal surfaces based object segmentation, IEEE-PAMI 19 (4) (1997) 394–398.
[22] V. Caselles, J.M. Morel, G. Sapiro, A. Tannenbaum (Eds.), Special Issue on Partial Differential Equations and Geometry-Driven Diffusion in Image Processing and Analysis, IEEE Trans. Image Process. 7 (1998).
[23] C. Cercignani, I. Gamba, J. Jerome, C.-W. Shu, Device benchmark comparisons via kinetic, hydrodynamic, and high-field models, Comput. Methods Appl. Mech. Eng. 181 (2000) 381–392.
[24] S. Chakravarthy, S. Osher, Numerical experiments with the Osher upwind scheme for the Euler equations, AIAA J. 21 (1983) 1241–1248.
[25] T.F. Chan, G.H. Golub, P. Mulet, A nonlinear primal-dual method for total variation-based image restoration, SIAM J. Sci. Comput. 20 (1999) 1964–1977.
[26] T. Chan, L. Vese, Active contour model without edges, in: M. Neilsen, P. Johansen, O.F. Olson, J. Weickert (Eds.), Lecture Notes in C.S., vol. 1687, Springer-Verlag, Berlin/New York, 1999, p. 141.
[27] T. Chan, L. Vese, A level set algorithm for minimizing the Mumford–Shah functional in image processing, in: Proceedings of the 1st IEEE Workshop on "Variational and Level Set Methods in Computer Vision", 2001, pp. 161–168.
[28] T. Chan, C.K. Wong, Total variation blind deconvolution, IEEE Trans. Image Process. 7 (1998) 370–375.
[29] Y. Chang, T. Hou, B. Merriman, S. Osher, A level set formulation of Eulerian interface capturing methods for incompressible fluid flows, J. Comput. Phys. 124 (1996) 449–464.
[30] S. Chen, B. Merriman, M. Kang, R. Caflisch, C. Ratsch, M. Guyre, R. Fedkiw, C. Anderson, S. Osher, A level set method for thin film epitaxial growth, J. Comput. Phys. 167 (2001) 475–500.
[31] S. Chen, B. Merriman, S. Osher, P. Smereka, A simple level set method for solving Stefan problems, J. Comput. Phys. 135 (1997) 8–29.
[32] Y.G. Chen, Y. Giga, S. Goto, Uniqueness and existence of viscosity solutions of generalized mean curvature flow equations, J. Differential Geom. 33 (1991) 749–786.
[33] L.-T. Cheng, P. Burchard, B. Merriman, S. Osher, Motion of curves constrained on surfaces using a level set approach, J. Comput. Phys. 175 (2002) 604–644.
[34] D. Chopp, Computing minimal surfaces via level set curvature flow, J. Comput. Phys. 106 (1993) 77–91.
[35] A. Cohen, W. Dahmen, I. Daubechies, R. DeVore, Harmonic analysis of the space BV, Acta Math. (2000), submitted.
[36] P. Colella, A. Majda, V. Roytburd, Theoretical and numerical structure for reacting shock waves, SIAM J. Sci. Comput. 7 (1986) 1059–1080.
[37] M. Crandall, P.-L. Lions, Viscosity solutions of Hamilton–Jacobi equations, Trans. Amer. Math. Soc. 277 (1983) 1–42.
[38] M. Crandall, P.-L. Lions, Two approximations of solutions of Hamilton–Jacobi equations, Math. Comp. 43 (1984) 1–19.
[39] M. Crandall, A. Majda, Monotone difference approximations for scalar conservation laws, Math. Comput. 34 (1980) 1–21.
[40] U. Diewald, T. Preufer, M. Rumpf, Anisotropic diffusion in vector field visualization on Euclidean domains and surfaces, IEEE Trans. Visual. Comput. Graph. 6 (2000) 139–149.
[41] J. Dorsey, P. Hanrahan, Digital materials and virtual weathering, Sci. Amer. 282 (2) (2000) 46–53.
[42] L.J. Durlofsky, B. Engquist, S. Osher, Triangle based adaptive stencils for the solution of hyperbolic conservation laws, J. Comput. Phys. 98 (1992) 64–73.

[43] M. Eck, T. DeRose, T. Duchamp, H. Hoppe, M. Lounsbery, W. Stuetzle, Multi-resolution analysis of arbitrary meshes, Comput. Graph. (SIGGRAPH '95 Proc.) (1995) 173–182.
[44] M. Eck, H. Hoppe, Automatic reconstruction of B-spline surfaces of arbitrary topological type, Comput. Graph. (1996).
[45] J. Eells, L. Lemarie, A report on harmonic maps, Bull. London Math. Soc. 10 (1) (1978) 1–68.
[46] B. Engquist, E. Fatemi, S. Osher, Numerical solution of the high frequency asymptotic expansion for hyperbolic equations, in: Proc. 10th Ann. Review of Progress in Applied Comp. Electromagnetics, Monterey, CA, 1994, pp. 32–45.
[47] B. Engquist, S. Osher, Stable and entropy satisfying approximations for transonic flow calculations, Math. Comp. 34 (1980) 45–57.
[48] B. Engquist, S. Osher, One-sided difference approximations for nonlinear conservation laws, Math. Comp. 36 (1981) 321–351.
[49] B. Engquist, S. Osher, S. Zhong, Fast wavelet based algorithms for linear evolution equations, SIAM J. Sci. Statist. Comput. 15 (4) (1994) 755–775.
[50] B. Engquist, O. Runborg, A.-K. Tornberg, High frequency wave propagation by the segment projection method, J. Comput. Phys. 178 (2002) 373–390.
[51] D. Enright, R. Fedkiw, J. Ferziger, I. Mitchell, A hybrid particle level set method for improved interface capturing, J. Comput. Phys. 183 (2002) 83–116.
[52] D. Enright, S. Marschner, R. Fedkiw, Animation and rendering of complex water surfaces, in: Siggraph 2002 Annual Conference, ACM TOG, 21, 2002, pp. 736–744.
[53] L.C. Evans, Convergence of an algorithm for mean curvature motion, Indiana Univ. Math. J. 42 (1993) 553–557.
[54] L.C. Evans, J. Spruck, Motion of level sets by mean curvature, I, J. Differential Geom. 33 (1991) 635–681.
[55] E. Fatemi, B. Engquist, S. Osher, Numerical solution of the high frequency asymptotic expansion of the scalar wave equation, J. Comput. Phys. 120 (1995) 145–155.
[56] E. Fatemi, B. Engquist, S. Osher, Finite difference methods for the nonlinear equations of perturbed geometric optics, ACES J. 11 (1996) 90–98.
[57] E. Fatemi, J. Jerome, S. Osher, Solution of the hydrodynamic device model using high order nonoscillatory shock capturing algorithms, IEEE Trans. Comput.-Aided Design Integrated Circ. Syst. 10 (1991) 232–243.
[58] O. Faugeras, F. Clément, R. Deriche, R. Keriven, T. Papadopoulo, J. Gomes, G. Hermosillo, P. Kornprobst, D. Lingrad, J. Roberts, T. Viéville, F. Devernay, The inverse EEG and MEG problems: the adjoint state approach I – The continuous case, INRIA Research Report 3673, June 1999.
[59] R. Fedkiw, Coupling an Eulerian fluid calculation to a Lagrangian solid calculation with the ghost fluid method, J. Comput. Phys. 175 (2002) 200–224.
[60] R. Fedkiw, T. Aslam, B. Merriman, S. Osher, A non-oscillatory Eulerian approach to interfaces in multimaterial flows (the ghost fluid method), J. Comput. Phys. 152 (1999) 457–492.
[61] R. Fedkiw, T. Aslam, S. Xu, The ghost fluid method for deflagration and detonation discontinuities, J. Comput. Phys. 154 (1999) 393–427.
[62] R. Fedkiw, B. Merriman, S. Osher, High accuracy numerical methods for thermally perfect gas flows with chemistry, J. Comput. Phys. 132 (1997) 175–190.
[63] R. Fedkiw, B. Merriman, S. Osher, Efficient characteristic projection in upwind difference schemes for hyperbolic systems; the complementary projection method, J. Comput. Phys. 141 (1998) 22–36.
[64] N. Foster, R. Fedkiw, Practical animation of liquids, in: Siggraph 2001 Annual Conference, 2001, pp. 15–22.
[65] S.F. Frisken, R.N. Perry, A. Rockwood, T. Jones, Adaptively sampled fields: A general representation of shape for computer graphics, in: Computer Graphics (SIGGRAPH), New Orleans, July 2000.
[66] D. Gabor, Information theory in electron microscopy, Lab. Invest. 14 (1965) 801–807.
[67] Y. Giga, M.-H. Sato, A level set approach to semicontinuous solutions for Cauchy problems, Commun. Partial Differential Equations 26 (2001) 813–839.
[68] J. Glimm, L. Xia, Y. Liu, N. Zhao, Conservative front tracking and level set algorithms, PNAS 98 (2001) 14198–14201.
[69] S. Gottlieb, C.-W. Shu, E. Tadmor, Strong stability preserving high order time discretization methods, SIAM Rev. 43 (2001) 89–112.
[70] M. Grayson, The heat equation shrinks embedded plane curves to round points, J. Differential Geom. 26 (1987) 285–314.
[71] M. Green, S. Osher, Steiner polynomials, Wulff flows and some new isoperimetric inequalities for convex plane curves, Asian J. Math. 3 (1999) 659–676.
[72] F. Guichard, J.M. Morel, Introduction to Partial Differential Equations in Image Processing, Tutorial Notes, IEEE Int. Conf. Image Proc., Washington, DC, October 1995.
[73] B. Gustafsson, H.-O. Kreiss, A. Sundstrom, Stability theory of difference approximations for mixed initial boundary value problems. II, Math. Comp. 26 (1972) 649–686.
[74] M. Gyure, C. Ratsch, B. Merriman, R. Caflisch, S. Osher, J. Zinck, D. Vvedensky, Level set methods for the simulation of epitaxial phenomena, Phys. Rev. E. 58 (1998) 6927–6930.

[75] E. Harabetian, S. Osher, Regularization of ill-posed problems via the level set approach, SIAM J. Appl. Math. 58 (1998) 1689–1706.
[76] E. Harabetian, S. Osher, C.-W. Shu, An Eulerian approach for vortex motion using a level set regularization procedure, J. Comput. Phys. 127 (1996) 15–26.
[77] A. Harten, High resolution schemes for hyperbolic conservation laws, J. Comput. Phys. 49 (1983) 357–393.
[78] A. Harten, B. Engquist, S. Osher, S. Chakravarthy, Uniformly high-order accurate essentially non-oscillatory schemes III, J. Comput. Phys. 71 (1987) 231–303.
[79] A. Harten, S. Osher, Uniformly high-order accurate non-oscillatory schemes, I, SIAM J. Numer. Anal. 24 (1987) 279–304.
[80] A. Harten, S. Osher, B. Engquist, S. Chakravarthy, Some results on uniformly high order accurate essentially non-oscillatory schemes, Appl. Numer. Math. 2 (1986) 347–377.
[81] J. Helmsen, E. Puckett, P. Colella, M. Dorr, Two new methods for simulating photolithography development in 3D, Proc. SPIE 2726 (1996) 253–261.
[82] C. Hu, C.-W. Shu, Weighted essentially non-oscillatory schemes on triangular meshes, J. Comput. Phys. 150 (1999) 97–127.
[83] G. Huiskamp, Difference formulas for the surface Laplacian on a triangulated surface, J. Comput. Phys. 95 (1991) 477–496.
[84] R.A. Hummel, Representations based on zero-crossings in scale-space, Proc. IEEE CVPR (1986) 204–209.
[85] H. Ishii, A generalization of Bence, Merriman, and Osher algorithm for motion by mean curvature, in: A. Damlamian, J. Spruck, A. Visintin (Eds.), Curvature Flows and Related Topics, Gakkôtosho, Tokyo, 1995, pp. 111–127.
[86] H. Ishii, G.E. Pires, P.E. Souganidis, Threshold dynamics type schemes for propagating fronts, J. Math. Soc. Jpn. 51 (2) (1999) 267–308.
[87] A.K. Jain, Partial differential equations and finite-difference methods in image processing, Part 1: Image representation, J. Optim. Theory Appl. 23 (1977) 65–91.
[88] J. Jerome, C.-W. Shu, Transport effects and characteristic modes in the modeling and simulation of submicron devices, IEEE Trans. Comput.-Aided Design Integrated Circ. Syst. 14 (1995) 917–923.
[89] G.-S. Jiang, D. Peng, Weighted ENO schemes for Hamilton Jacobi equations, SIAM J. Sci. Comput. 21 (2000) 2126–2143.
[90] G.-S. Jiang, C.-W. Shu, Efficient implementation of weighted ENO schemes, J. Comput. Phys. 126 (1996) 202–228.
[91] M. Kang, R. Fedkiw, X.-D. Liu, A boundary condition capturing method for multiphase incompressible flow, J. Sci. Comput. 15 (2000) 323–360.
[92] S. Karni, Multicomponent flow calculations by a consistent primitive algorithm, J. Comput. Phys. 112 (1994) 31–43.
[93] M. Kass, A. Witkin, D. Terzopoulos, Snakes: Active contour models, Int. J. Comput. Vision 1 (1988) 321–331.
[94] S. Kichenassamy, A. Kumar, P. Olver, A. Tannenbaum, A. Yezzi, Conformal curvature flows: from phase transitions to active vision, Arch. Rational Mech. Anal. 134 (1996) 275–301.
[95] Y.-T. Kim, N. Goldenfeld, J. Dantzig, Computation of dendritic microstructures using a level set method, Phys. Rev. E 62 (2000) 2471–2474.
[96] B.B. Kimia, A. Tannenbaum, S.W. Zucker, Toward a computational theory of shape: an overview, in: Lecture Notes in Computer Science, 427, Springer-Verlag, New York, 1990, pp. 402–407.
[97] R. Kimmel, Numerical geometry of images: theory, algorithms, and applications, Technion CIS Report 9910, October 1999.
[98] R. Kimmel, A.M. Bruckstein, Tracking level sets by level sets: a method for solving the shape from shading problem, CVIU 62 (1) (1995) 47–58.
[99] J.J. Koenderink, The structure of images, Biol. Cybernet. 50 (1984) 363–370.
[100] H.-O. Kreiss, Difference approximations for the initial-boundary value problem for hyperbolic differential equations, in: D. Greenspan (Ed.), Numerical Solutions of Nonlinear Differential Equations, Wiley, New York, 1966, pp. 141–166.
[101] F. Lafon, S. Osher, High order two dimensional nonoscillatory methods for solving Hamilton–Jacobi equations, J. Comput. Phys. 123 (1996) 235–253.
[102] R. Lagnado, S. Osher, Reconciling differences, Risk Mag. 10 (1997) 79–83.
[103] R. Lagnado, S. Osher, A technique for calibrating derivative security pricing models, numerical solution of an inverse problem, J. Comput. Finance 1 (1997) 13–25.
[104] T. Lindeberg, Scale-Space Theory in Computer Vision, Kluwer Academic Publishers, Dordrecht, 1994.
[105] X.-D. Liu, R. Fedkiw, M. Kang, A boundary condition capturing method for Poisson's equation on irregular domains, J. Comput. Phys. 160 (2000) 151–178.
[106] X.-D. Liu, S. Osher, Nonoscillatory high order accurate self similar maximum principle satisfying shock capturing schemes, SIAM J. Numer. Anal. 33 (1996) 760–779.
[107] X.-D. Liu, S. Osher, Convex ENO high-order multidimensional schemes without field by field projection or staggered grids, J. Comput. Phys. 142 (1998) 304–330.
[108] X.-D. Liu, S. Osher, T. Chan, Weighted essentially non-oscillatory schemes, J. Comput. Phys. 115 (1994) 200–212.
[109] A. Majda, J. McDonough, S. Osher, The Fourier method for nonsmooth initial data, Math. Comp. 32 (1978) 1041–1081.
[110] A. Majda, S. Osher, Reflections of singularities at the boundary, Commun. Pure Appl. Math. 28 (1975) 479–499.

[111] A. Majda, S. Osher, Initial-boundary value problems for hyperbolic equations with uniformly characteristic boundary, Commun. Pure Appl. Math. 28 (1975) 607–675.
[112] A. Majda, S. Osher, Propagation of error into regions of smoothness for accurate difference approximations to hyperbolic equations, Commun. Pure Appl. Math. 30 (1977) 671–705.
[113] A. Majda, S. Osher, A systematic approach for correcting nonlinear instabilities: the Lax–Wendroff scheme for scalar conservation laws, Numer. Math. 30 (1978) 429–452.
[114] R. Malladi, J.A. Sethian, B.C. Vemuri, Evolutionary fronts for topology independent shape modeling and recovery, in: Proc. of the 3rd ECCV, Stockholm, Sweden, 1994, pp. 3–13.
[115] R. Malladi, J.A. Sethian, B.C. Vemuri, Shape modeling with front propagation: a level set approach, IEEE Trans. PAMI 17 (1995) 158–175.
[116] A. Marquina, S. Osher, Explicit algorithms for a new time dependent model based on level set motion for nonlinear debluring and noise removal, SIAM J. Sci. Comput. 22 (2000) 387–405.
[117] T. McInerney, D. Terzopoulos, Topologically adaptable snakes, in: Proc. ICCV, Cambridge, MA, June 1995.
[118] B. Merriman, J. Bence, S. Osher, Diffusion generated motion by mean curvature, in: J.E. Taylor (Ed.), Computational Crystal Growers Workshop, American Mathematical Society, Providence, RI, 1992, pp. 73–83.
[119] B. Merriman, J. Bence, S. Osher, Motion of multiple junctions: a level-set approach, J. Comput. Phys. 112 (1994) 334–363.
[120] B. Merriman, R. Caflisch, S. Osher, Level set methods with an application to modeling the growth of thin films, in: I. Athanasopoulos, G. Makreakis, J. Rodrigues (Eds.), Free Boundary Value Problems, Theory and Applications, CRC Press, Boca Raton, 1999, pp. 51–70.
[121] W. Mulder, S. Osher, J. Sethian, Computing interface motion in compressible gas dynamics, J. Comput. Phys. 100 (1992) 209–228.
[122] D. Mumford, J. Shah, Optimal approximations by piecewise smooth functions and variational problems, Commun. Pure Appl. Math. 42 (1989) 577–685.
[123] D. Nguyen, R. Fedkiw, H. Jensen, Physically based modeling and animation of fire, in: Siggraph 2002 Annual Conference, ACM TOG, 21, 2002, pp. 721–728.
[124] D. Nguyen, R. Fedkiw, M. Kang, A boundary condition capturing method for incompressible flame discontinuities, J. Comput. Phys. 172 (2001) 71–98.
[125] D. Nguyen, F. Gibou, R. Fedkiw, A fully conservative ghost fluid method and stiff detonation waves, 12th International Detonation Symposium, San Diego, CA, 2002.
[126] J. Oliensis, P. Dupuis, Direct method for reconstructing shape from shading, in: Proceedings SPIE Conf. 1570 on Geometric Methods in Computer Vision, 1991, pp. 116–128.
[127] S. Osher, Systems of difference equations with general homogeneous boundary conditions, Trans. Amer. Math. Soc. 137 (1969) 177–201.
[128] S. Osher, Stability of parabolic difference approximations to certain mixed initial boundary value problems, Math. Comp. 26 (1972) 13–39.
[129] S. Osher, Numerical solution of singular perturbation problems and one-sided difference schemes, North-Holland Math. Stud. 47 (1981).
[130] S. Osher, The Riemann problem for nonconvex scalar conservation laws and the Hamilton–Jacobi equations, Proc. Amer. Math. Soc. 89 (1983) 641–646.
[131] S. Osher, Riemann solvers, the entropy condition and difference approximations, SIAM J. Numer. Anal. 21 (1984) 217–235.
[132] S. Osher, Convergence of generalized MUSCL schemes, SIAM J. Numer. Anal. 22 (1985) 947–961.
[133] S. Osher, A level set formulation for the solution of the Dirichlet problem for Hamilton–Jacobi equations, SIAM J. Anal. 24 (1993) 1145–1152.
[134] S. Osher, S. Chakravarthy, Upwind schemes and boundary conditions with applications to Euler equations in general geometries, J. Comput. Phys. 50 (1983) 447–481.
[135] S. Osher, S. Chakravarthy, High resolution schemes and the entropy condition, SIAM J. Numer. Anal. 21 (1984) 955–984.
[136] S. Osher, S. Chakravarthy, Very high order accurate TVD schemes, in: IMA Volumes in Mathematics and Its Applications, 2, Springer-Verlag, New York, 1986, pp. 229–274.
[137] S. Osher, L.-T. Cheng, M. Kang, H. Shim, Y.-H. Tsai, Geometric optics in a phase space and Eulerian framework, J. Comput. Phys., to appear.
[138] S. Osher, R. Fedkiw, Level set methods: an overview and some recent results, J. Comput. Phys. 169 (2001) 463–502.
[139] S. Osher, R. Fedkiw, Level sets and dynamic implicit surfaces, Springer-Verlag, New York, 2002.
[140] S. Osher, M. Hafez, W. Whitlow Jr., Entropy condition satisfying approximations for the full potential equation of transonic flow, Math. Comp. 44 (1985) 1–29.
[141] S. Osher, B. Merriman, The Wulff shape as the asymptotic limit of a growing crystalline interface, Asian J. Math. 1 (1997) 560–571.
[142] S. Osher, R.T. Rudin, Feature-oriented image enhancement using shock filters, SIAM J. Numer. Anal. 27 (1990) 919–940.

[143] S. Osher, R. Sanders, Numerical approximations to nonlinear conservation laws with locally varying time and space grids, Math. Comp. 41 (1983) 321–336.
[144] S. Osher, F. Santosa, Level set method for optimization problems involving geometry and constraints, I. Frequencies of a two-density inhomogeneous drum, J. Comput. Phys. 171 (2001) 277–288.
[145] S. Osher, J. Sethian, Fronts propagating with curvature dependent speed: algorithms based on Hamilton–Jacobi formulations, J. Comput. Phys. 79 (1988) 12–49.
[146] S. Osher, C.-W. Shu, High order essentially non-oscillatory schemes for Hamilton–Jacobi equations, SIAM J. Numer. Anal. 28 (1991) 902–921.
[147] S. Osher, F. Solomon, Upwind difference schemes for hyperbolic systems of conservation laws, Math. Comp. 38 (1982) 339–374.
[148] S. Osher, E. Tadmor, On the convergence of difference approximations to scalar conservation laws, Math. Comp. 50 (1988) 19–51.
[149] N. Paragios, R. Deriche, A PDE-based level-set approach for detection and tracking of moving objects, in: Proc. Int. Conf. Comp. Vision '98, Bombay, India, January 1998.
[150] D. Peng, B. Merriman, S. Osher, H.-K. Zhao, M. Kang, A PDE-based fast local level set method, J. Comput. Phys. 155 (1999) 410–438.
[151] D. Peng, S. Osher, B. Merriman, H.-K. Zhao, The geometry of Wulff crystal shapes and its relations with Riemann problems, in: G.Q. Chen, E. DeBenedetto (Eds.), Contemp. Math., vol. 238, American Mathematical Society, Providence, RI, 1999, p. 251.
[152] P. Perona, J. Malik, Scale-space and edge detection using anisotropic diffusion, IEEE Trans. Pattern Anal. Machine Intell. 12 (1990) 629–639.
[153] E. Praun, A. Finkelstein, H. Hoppe, Lapped textures, ACM Computer Graphics (SIGGRAPH), New Orleans, July 2000.
[154] C.B. Price, P. Wambacq, A. Oosterlink, Image enhancement and analysis with reaction–diffusion paradigm, IEE Proc. 137 (1990) 136–145.
[155] B. Romeny (Ed.), Geometry Driven Diffusion in Computer Vision, Kluwer Academic Publishers, Dordrecht, 1994.
[156] E. Rouy, A. Tourin, A viscosity solutions approach to shape-from-shading, SIAM J. Numer. Anal. 29 (1992) 867–884.
[157] L.I. Rudin, S. Osher, E. Fatemi, Nonlinear total variation based noise removal algorithms, Physica D 60 (1992) 259–268.
[158] S. Ruuth, B. Merriman, S. Osher, Convolution generated motion as a link between cellular automata and continuum pattern dynamics, J. Comput. Phys. 151 (1999) 836–861.
[159] S. Ruuth, B. Merriman, S. Osher, A fixed grid method for capturing the motion of self-intersecting interfaces and related PDEs, J. Comput. Phys. 163 (2000) 1–21.
[160] S. Ruuth, B. Merriman, J. Xin, S. Osher, A diffusion generated approach to the curvature motion of filaments, J. Nonlinear Sci. 61 (2001) 473–494.
[161] G. Sapiro, Geometric Partial Differential Equations and Image Processing, Cambridge University Press, New York, 2001.
[162] J. Serra, Image Analysis and Mathematical Morphology, vol. 2: Theoretical Advances, Academic Press, New York, 1988.
[163] J.A. Sethian, Level Set Methods: Evolving Interfaces in Geometry, Fluid Mechanics, Computer Vision, and Materials Sciences, Cambridge University Press, Cambridge, UK, 1996.
[164] J.A. Sethian, A fast marching method for three dimensional photolithography development, in: Proc. SPIE, 2726, 1996, p. 261.
[165] J. Shah, A common framework for curve evolution, segmentation, and anisotropic diffusion, in: Proc. CVPR, San Francisco, June 1996.
[166] J. Shi, C. Hu, C.-W. Shu, A technique of treating negative weights in WENO schemes, J. Comput. Phys. 175 (2002) 108–127.
[167] C.-W. Shu, Essentially non-oscillatory and weighted essentially non-oscillatory schemes for hyperbolic conservation laws, in: B. Cockburn, C. Johnson, C.-W. Shu, E. Tadmor (Editor: A. Quarteroni), Advanced Numerical Approximation of Nonlinear Hyperbolic Equations, Lecture Notes in Mathematics, vol. 1697, Springer, Berlin, 1998, pp. 325–432.
[168] C.-W. Shu, S. Osher, Efficient implementation of essentially non-oscillatory shock capturing schemes, J. Comput. Phys. 77 (1988) 439–471.
[169] C.-W. Shu, S. Osher, Efficient implementation of essentially non-oscillatory shock capturing schemes II, J. Comput. Phys. 83 (1989) 32–78.
[170] C.-W. Shu, T.A. Zang, G. Erlebacher, D. Whitaker, S. Osher, High-order ENO schemes applied to two- and three-dimensional compressible flow, Appl. Numer. Math. 9 (1992) 45–71.
[171] L. Simon, Lectures on Geometric Measure Theory, Australian National University, Australia, 1984.
[172] J. Steinhoff, M. Fang, L. Wang, A new Eulerian method for the computation of propagating short acoustic and electromagnetic pulses, J. Comput. Phys. 157 (2000) 683–706.
[173] M. Struwe, On the evolution of harmonic mappings of Riemannian surfaces, Comment. Math. Helv. 60 (1985) 558–581.
[174] M. Sussman, P. Smereka, S. Osher, A level set approach for computing solutions to incompressible two-phase flow, J. Comput. Phys. 114 (1994) 146–159.
[175] B. Tang, G. Sapiro, V. Caselles, Diffusion of general data on non-flat manifolds via harmonic maps theory: the direction diffusion case, Int. J. Comput. Vision 36 (2) (2000) 149–161.
[176] G. Taubin, Estimation of planar curves, surfaces, and nonplanar space curves defined by implicit equations with applications to edge and range image segmentation, IEEE Trans. PAMI 13 (11) (1991) 1115–1138.

[177] H. Tek, B.B. Kimia, Image segmentation by reaction–diffusion bubbles, in: Proc. ICCV'95, Cambridge, June, 1995, pp. 156–162.
[178] A.W. Toga, Brain Warping, Academic Press, New York, 1998.
[179] V.T. Ton, A.R. Karagozian, S. Osher, B. Engquist, Numerical simulation of high speed chemically reactive flow, Theoret. Comput. Fluid Dyn. 6 (1994) 161–179.
[180] Y.-H. Tsai, Y. Giga, S. Osher, A level set approach for computing discontinuous solutions of Hamilton–Jacobi equations, Math. Comp., to appear.
[181] J. Tsitsiklis, Efficient algorithms for globally optimal trajectories, in: Proceedings of the 33rd Conference on Decision and Control, Lake Buena Vista, LF, December, 1994, pp. 1368–1373.
[182] J. Tsitsiklis, Efficient algorithms for globally optimal trajectories, IEEE Trans. Automat. Control 40 (1995) 1528–1538.
[183] A. Turing, The chemical basis of morphogenesis, Philos. Trans. Roy. Soc. B 237 (1952) 37–72.
[184] G. Turk, Generating textures on arbitrary surfaces using reaction–diffusion, Comput. Graph. 25 (4) (1991) 289–298.
[185] B. van Leer, Towards the ultimate conservative difference scheme V. A second order sequel to Godunov's method, J. Comput. Phys. 32 (1979) 101–136.
[186] J. Varah, Stability of difference approximations to the mixed initial boundary value problem for parabolic systems, SIAM J. Numer. Anal. 8 (1971) 598–615.
[187] L.A. Vese, T.F. Chan, A multiphase level set framework for image segmentation using the Mumford and Shah model, Int. J. Comp. Vision 50 (3) (2002) 271–293.
[188] J. Weickert, Anisotropic Diffusion in Image Processing, ECMI Series, Teubner, Stuttgart, Germany, 1998.
[189] R.T. Whitaker, Algorithms for implicit deformable models, in: Proc. ICCV'95, Cambridge, June, 1995, pp. 822–827.
[190] G. Winkenbach, D.H. Salesin, Rendering parametric surfaces in pen and ink, Comput. Graph. (SIGGRAPH 96) (1996) 469–476.
[191] A.P. Witkin, Scale-space filtering, Int. Joint Conf. Artif. Intell. 2 (1983) 1019–1021.
[192] A. Witkin, P. Heckbert, Using particles to sample and control implicit surfaces, Comput. Graph. (SIGGRAPH) (1994) 269–278.
[193] A. Witkin, M. Kass, Reaction–diffusion textures, Comput. Graph. (SIGGRAPH) 25 (4) (1991) 299–308.
[194] A. Yezzi, S. Soatto, Stereoscopic segmentation, in: IEEE Intl. Conf. on Computer Vision, Vancouver, July, 2001, pp. 59–66.
[195] Y.-T. Zhang, C.-W. Shu, High order WENO schemes for Hamilton–Jacobi equations on triangular meshes, SIAM J. Sci. Comput., to appear.
[196] H.-K. Zhao, T. Chan, B. Merriman, S. Osher, A variational level set approach to multiphase motion, J. Comput. Phys. 127 (1996) 179–195.
[197] H.-K. Zhao, B. Merriman, S. Osher, C. Wang, Capturing the behavior of bubbles and drops using the variational level set approach, J. Comput. Phys. 143 (1998) 495.
[198] H.-K. Zhao, S. Osher, R. Fedkiw, Fast surface reconstruction using the level set method, in: 1st IEEE Workshop on Variational and Level Set Methods, in conjunction with the 8th International Conference on Computer Vision (ICCV), Vancouver, Canada, 2001, pp. 194–202.
[199] H.-K. Zhao, S. Osher, B. Merriman, M. Kang, Implicit nonparametric shape reconstruction from unorganized points using a variational level set method, Comput. Vision Image Understanding 80 (2000) 295–314.